

Aus der
Klinik und Poliklinik für Nuklearmedizin
Klinikum der Ludwig-Maximilians-Universität München
Direktor: Prof. Dr. Rudolf Alexander Werner

**Application, validation and optimization of antibody-based
TREM2 PET**

Dissertation
zum Erwerb des Doktorgrades der Naturwissenschaften
an der Medizinischen Fakultät der
Ludwig-Maximilians-Universität München

vorgelegt von
Rebecca Schäfer

aus
Köln

Jahr
2025

Mit Genehmigung der Medizinischen Fakultät
der Ludwig-Maximilians-Universität München

Betreuer: PD Dr. Simon Lindner

Zweitgutachter: PD Dr. Christian Thieke

Dekan: Prof. Dr. med. Thomas Gudermann

Tag der mündlichen Prüfung: 06. März 2026

Übereinstimmungserklärung



Erklärung zur Übereinstimmung der gebundenen Ausgabe der Dissertation mit der elektronischen Fassung

Schäfer, Rebecca

Name, Vorname

Hiermit erkläre ich, dass die elektronische Version der eingereichten Dissertation mit dem Titel:

Application, validation and optimization of antibody-based TREM2 PET

in Inhalt und Formatierung mit den gedruckten und gebundenen Exemplaren übereinstimmt.

München, 07.03.2026

Ort, Datum

Rebecca Schäfer

Unterschrift Doktorandin bzw. Doktorand

Affidavit



Dekanat Medizinische Fakultät
Promotionsbüro



Eidesstattliche Versicherung

Schäfer, Rebecca

Name, Vorname

Ich erkläre hiermit an Eides statt, dass ich die vorliegende Dissertation mit dem Titel:

Application, validation and optimization of antibody-based TREM2 PET

selbständig verfasst, mich außer der angegebenen keiner weiteren Hilfsmittel bedient und alle Erkenntnisse, die aus dem Schrifttum ganz oder annähernd übernommen sind, als solche kenntlich gemacht und nach ihrer Herkunft unter Bezeichnung der Fundstelle einzeln nachgewiesen habe.

Ich erkläre des Weiteren, dass die hier vorgelegte Dissertation nicht in gleicher oder in ähnlicher Form bei einer anderen Stelle zur Erlangung eines akademischen Grades eingereicht wurde.

München, 07.03.2026

Ort, Datum

Rebecca Schäfer

Unterschrift Doktorandin bzw. Doktorand

Declaration of the Use of Artificial Intelligence

The artificial intelligence-assisted technology *ChatGPT* (version 4.0, OpenAI) was employed to enhance the language and readability of the dissertation. The author throughout reviewed and revised the results, taking full responsibility for its content.

No generative artificial intelligence was used in the process of preparing this dissertation.

Table of Contents

Übereinstimmungserklärung	iii
Affidavit.....	4
Declaration of the Use of Artificial Intelligence.....	5
Table of Contents	vi
Abbreviations	viii
1. Abstract	1
2. Zusammenfassung	4
3. Introduction	7
3.1 AD and the Role of Microglia.....	8
3.2 TREM2 Biology and Imaging Potential	9
3.3 Molecular Imaging of Neuroinflammation.....	10
3.4 Considerations for the Development of Antibody-based TREM2 PET Radioligands	14
3.5 Improved Quantification Strategies for TREM2 PET	18
3.6 Aims.....	20
4. Content of the Doctoral Thesis	22
4.1 Targeting Microglia in AD: A PET Imaging Approach with Copper-64 labeled TREM2 Antibodies	22
4.2 Enhancing Quantitative Analysis of TREM2 PET Imaging: Image-Derived Blood Normalization in Mouse Models.....	29
5. Conclusion and Outlook	36
6. Publications.....	38
6.1 List of Publications	38
6.2 Contribution to Paper I.....	42
6.3 Contribution to the Paper II.....	44
7. Bibliography	46
8. List of Figures	59
9. List of Tables.....	61
10. Paper I.....	62

11. Paper II	63
Danksagung	64

Abbreviations

A β	Amyloid-beta
AD	Alzheimer's disease
ADAM10/17	Disintegrin and metalloproteinase domain-containing protein 10/17
APP	Amyloid beta precursor protein
<i>APP^{SAA}</i>	Amyloid beta precursor protein with the Swedish (KM670/671NL), Arctic (E693G), and Austrian (T714I) mutation
<i>APP^{SAA};TfR^{mu/hu}</i>	B6(Cg)-App ^{tm1.1Dnli} /J, homozygous for <i>APP^{SAA}</i> , homozygous for hTfR
ATV	Antibody Transport Vehicle
BBB	Blood-brain barrier
CD11b	Cluster of differentiation 11b
CNS	Central nervous system
CT	Computed tomography
DAP10	DNAX-activating protein 10
DAP12	DNAX-activating protein of 12 kDa
ERK	Extracellular-signal-regulated kinase
FAD	Familial Alzheimer's disease
hTfR	Human transferrin receptor
IgG	Immunoglobulin G
KI	Knock-in
KO	Knock-out
LAD	Left anterior descending artery
MSD	Meso Scale Discovery
NMDA	<i>N</i> -methyl-D-aspartate
PET	Positron emission tomography
p.i.	Post-injection
PI3K	Phosphatidylinositol 3-kinase
<i>p</i> -NCS-benzyl-NODAGA	2,2'-(7-(1-carboxy-4-((4-isothiocyanatobenzyl)amino)-4-oxobutyl)-1,4,7-triazonane-1,4-diyl)diacetic acid
PSEN1/2	Presenilin 1/2
scFv	Single chain variable fragment

scRadiotracing	Single-cell radiotracing
SDS-PAGE	Sodium dodecyl sulfate-polyacrylamide gel electrophoresis
SPM	Statistical Parametric Mapping
sTREM2	Soluble TREM2
SUV	Standardized uptake value
SYK	Spleen tyrosine kinase
TfR1	Transferrin receptor 1
TREM2	Triggering Receptor Expressed on Myeloid Cells 2
TREM2 KO	TREM2 knock-out
TSPO	Translocator protein
VOI(s)	Volume(s)-of-interest
WT	C57BL/6J, "wild-type"
WT;TfR ^{mu/hu}	C57BL/6J, homozygous for hTfR
%ID	Percentage of injected dose
%ID/g	Percentage of injected dose per gram (or cubic centimeter) of tissue
[¹¹ C]PBR28	<i>N</i> -Acetyl- <i>N</i> -(2-[¹¹ C]methoxybenzyl)-2-phenoxy-5-pyridinamine
(<i>R</i>)-[¹¹ C]PK11195	(<i>R</i>)- <i>N</i> -([¹¹ C]methyl)- <i>N</i> -(1-methylpropyl)-1-(2-chlorophenyl)isoquinoline-3-carboxamide
[¹⁸ F]DPA-714	<i>N,N</i> -diethyl-2-[2-(4-(2-[¹⁸ F]fluoroethoxy)phenyl)-5,7-dimethylpyrazolo[1,5- <i>a</i>]pyrimidin-3-yl]acetamide
[¹⁸ F]GE-180	(4 <i>S</i>)- <i>N,N</i> -diethyl-9-[2-[¹⁸ F]fluoroethyl]-5-methoxy-2,3,4,9-tetrahydro-1 <i>H</i> -carbazole-4-carboxamide
5xFAD	B6.Cg-Tg(APPSwFILon,PSEN1*M146L*L286V)6799Vas/Mmjax
5xFAD;TfR ^{mu/hu}	B6.Cg-Tg(APPSwFILon,PSEN1*M146L*L286V)6799Vas/Mmjax, homozygous for hTfR

1. Abstract

Alzheimer's disease (AD) is among the most prevalent and socially impactful neurodegenerative diseases worldwide. One of the most significant pathophysiological alterations is the occurrence of microgliosis, defined as an immune reaction in which the central nervous system's (CNS) resident immune cells, microglia, respond to pathological processes, including the accumulation of amyloid deposits. This reaction generally manifests itself years prior to the clinical onset of initial symptoms. Consequently, the early and non-invasive detection of microglia activation holds considerable diagnostic and therapeutic potential. This could be used to assess the progression of the disease or to monitor immunomodulatory treatments.

Currently used radioligands, such as translocator protein (TSPO, 18 kDa)-targeting positron emission tomography (PET) radioligands, exhibit a limited cellular specificity. In contrast, the Triggering Receptor Expressed on Myeloid Cells 2 (TREM2) is a promising biomarker. It is expressed selectively in the CNS on microglia, playing a pivotal role in their activation. The objective of this doctoral thesis was to develop and preclinically validate a TREM2-specific, antibody-based PET radioligand. Furthermore, a methodology has been developed that facilitates enhanced quantification of TREM2-PET data through the implementation of image-derived blood normalization. This methodology has been validated through its application in two distinct disease models.

For this purpose, an antibody directed against murine TREM2 with (ATV:4D9) and without (4D9) integrated brain shuttle system was used. The ATV (Antibody Transport Vehicle) technology enables the radioligand to pass the blood-brain barrier (BBB) by interacting with the human transferrin receptor (hTfR). In the study, the antibodies were conjugated with the chelator 2,2'-(7-(1-carboxy-4-((4-isothiocyanatobenzyl)amino)-4-oxobutyl)-1,4,7-triazonane-1,4-diyl)diacetic acid (*p*-NCS-benzyl-NODAGA) and radiolabeled with copper-64. Subsequently, the antibodies were tested *in vitro* for radiochemical parameters, affinity and stability. PET imaging was performed in an AD mouse model (B6.Cg-Tg(APP^{Sw}FILon,PSEN1*^{M146L}*^{L286V})6799Vas/Mmjax, homozygous for hTfR; hereafter referred to as 5x^{FAD};TfR^{mu/hu}) with a wild-type control (C57BL/6J, homozygous for hTfR; hereafter referred to as WT;TfR^{mu/hu}) and hTfR-negative controls at three time-points: 2 h post-injection (p.i., early), 20 h p.i. (intermediate) and 40 h p.i. (late). For validation, *ex vivo* biodistribution analysis and autoradiography were performed. In addition, a cell type-specific investigation of signal origin was performed by single-cell radiotracing (scRadio-tracing) in another amyloidosis model (B6(Cg)-App^{tm1.1Dnl}/J, homozygous for the amyloid beta precursor protein with the Swedish (KM670/671NL), Arctic (E693G), and Austrian (T714I) mutations (APP^{SAA}), homozygous for hTfR; hereafter referred to as APP^{SAA};TfR^{mu/hu}). For human translation, a human-specific TREM2 antibody (14D3) was radiolabeled and tested in *post-mortem* brain slices from AD patients by *in vitro* autoradiography and validated against immunohistochemistry.

In the second study, we developed and validated a blood-level normalization strategy for antibody-based TREM2 PET imaging. Using PET scans from TREM2 knock-out (TREM2 KO) and C57BL/6J (henceforth designated as wild-type (WT)) mice injected with [⁶⁴Cu]Cu-NODAGA-ATV:4D9, image-derived blood activity was extracted from the heart and correlated with *ex vivo* blood levels using Statistical Parametric Mapping (SPM). This enabled the establishment of a voxel-wise normalization approach that improved inter-individual comparability of TREM2 PET signals. Validation was performed by correlating normalized PET signals with TREM2 protein levels in peripheral organs (bone marrow, liver, spleen, lung), measured using Meso Scale Discovery (MSD) technology. This approach was further tested across two different disease models (myocardial infarction and AD (*APP^{SAA};TfR^{mu/hu}*)), demonstrating utility for imaging TREM2 not only in the brain but also in peripheral organs, thereby broadening the potential applications of the radioligand.

The developed radioligands were obtained with high radiochemical purity (> 97.3%), radiochemical yield (> 67.1%), and specific activity (1.0-1.4 MBq/μg). Conjugation of the chelators to the ATV:4D9 antibody did not affect the agonistic potency toward the TREM2, and the stability of the radioligand was maintained over 48 h. Analysis of the PET and biodistribution data revealed that the 20 h p.i. PET time-point could be identified as optimal in terms of signal-to-noise ratio. The ATV technology enabled a 4.6-fold increased uptake of the radioligand [⁶⁴Cu]Cu-NODAGA-ATV:4D9 in the brain of hTfR-expressing mice. PET and autoradiography data showed significantly increased radioligand accumulation in microglia-rich regions of the cortex and hippocampus of AD mice compared to wild-type controls. The selective accumulation of radioligand in microglial cells (94.8%) was confirmed by scRadiotracing. In addition, the cellular uptake could explain the signal increase in the AD mouse model compared to the wild-type. *In vitro* autoradiography on human *post-mortem* brain tissue from patients with AD showed increased cortical binding of the human-specific radioligand (cortex-to-white matter ratio 2.4 ± 0.2 , median \pm SD), which was consistent with TREM2 immunohistochemistry (cortex-to-white matter ratio 2.4 ± 0.5 , median \pm SD).

The second study showed a significant correlation between the blood values extracted from PET images and the blood values obtained *ex vivo* ($R^2 = 0.9680$, $p < 0.0001$, linear regression). Image-based blood normalization proved to be more robust in detecting signal clusters in TREM2 PET compared to traditionally used percentage of injected dose (%ID) normalization. TREM2 signals from the group comparison correlated significantly with the measured TREM2 protein levels in the target organs ($R^2 = 0.7450$, $p < 0.0003$, linear regression). In disease models, TREM2-positive macrophages in the infarcted area of the heart and activated microglial cells in the AD model were reliably detected after blood normalization and correlated with signals from *ex vivo* autoradiography (myocardial infarction: $R^2 = 0.8584$, $p = 0.0001$; AD: $R^2 = 0.6902$, $p = 0.0008$, linear regression).

The results of this study show that [⁶⁴Cu]Cu-NODAGA-ATV:4D9 holds strong potential as a radioligand for the non-invasive *in vivo* visualization of TREM2-positive microglial cells. The combination of a specific targeting antibody and the use of ATV technology enables efficient brain

uptake and allows PET-based imaging of an antibody-based radioligand of TREM2 beyond the BBB for the first time. The quantitative evaluation of TREM2 PETs has significantly improved detection sensitivity and accuracy of true biological TREM2 expression by the newly established method of blood normalization.

TREM2 PET thus offers potential for early diagnosis of AD, improved monitoring of disease progression, and the accompanying evaluation of therapies, such as anti-amyloid- β therapies recently approved by the Food and Drug Administration and European Medicines Agency. In addition, other indications, such as glioblastoma and other chronic inflammatory diseases, could also benefit from TREM2 PET. The first clinical TREM2 PET trial has begun. The results of the clinical TREM2 PET examinations are expected soon and will provide decisive insights into the future potential of the molecular imaging method of TREM2 PET.

2. Zusammenfassung

Die Alzheimer-Erkrankung zählt zu den häufigsten und gesellschaftlich relevantesten neurodegenerativen Erkrankungen weltweit. Eine ihrer zentralen pathophysiologischen Veränderungen ist die Mikrogliose: Eine Immunreaktion, bei der die Mikrogliazellen, die residenten Immunzellen des zentralen Nervensystems, auf pathologische Prozesse wie Amyloidablagerungen reagieren. Diese Reaktion manifestiert sich in der Regel Jahre vor dem klinischen Auftreten erster Symptome. Eine frühzeitige, nicht-invasive Erfassung der Mikrogliaaktivierung wäre daher sowohl diagnostisch als auch therapeutisch von großem Wert. Diese könnte etwa zur Einschätzung des Krankheitsverlaufs oder zur Überwachung immunmodulierender Therapien genutzt werden.

Bisher eingesetzte Radioliganden, wie die gegen TSPO gerichteten PET-Radioliganden, weisen jedoch eine eingeschränkte zelluläre Spezifität auf. Der TREM2 stellt demgegenüber einen vielversprechenden Biomarker dar, da er im zentralen Nervensystem selektiv auf Mikrogliazellen exprimiert wird und eine zentrale Rolle bei deren Aktivierung spielt. Ziel dieser Promotionsarbeit war es daher, einen TREM2-spezifischen, antikörperbasierten PET-Radioliganden zu entwickeln und präklinisch zu validieren. Darüber hinaus wurde eine Methodik entwickelt, die eine verbesserte Quantifizierung der TREM2-PET-Daten mittels bildbasierter Blutnormalisierung ermöglicht. Diese Methodik wurde in zwei verschiedenen Krankheitsmodellen getestet.

Hierzu wurde ein gegen murinen TREM2 gerichteter Antikörper mit (ATV:4D9) und ohne (4D9) integriertem Brain-Shuttle-System genutzt. Die ATV-Technologie ermöglicht dem Radioliganden durch Interaktion mit dem humanen Transferrinrezeptor die Passage der Blut-Hirn-Schranke. Im Rahmen der Studie wurden die Antikörper mit dem Chelator *p*-NCS-benzyl-NODAGA konjugiert und mit Kupfer-64 radioaktiv markiert. In der Folge wurden die Antikörper hinsichtlich radiochemischer Parameter, Affinität und Stabilität *in vitro* geprüft. PET-Bildgebung wurde in einem Alzheimer-Mausmodell (5xFAD;TfR^{mu/hu}) mit einer Wildtyp-Kontrolle (WT;TfR^{mu/hu}) sowie hTfR-negativen Kontrollen an drei Zeitpunkten durchgeführt: 2 h p.i. (früh), 20 h p.i. (mittel) und 40 h p.i. (spät). Zur Validierung wurden *ex vivo* Biodistributionsanalysen und Autoradiographien durchgeführt. Darüber hinaus erfolgte eine zelltypspezifische Untersuchung der Signalherkunft durch scRadiotracing in einem weiteren Amyloidose-Modell (*APP*^{SAA};TfR^{mu/hu}). Zur humanen Translation wurde ein human-spezifischer TREM2-Antikörper (14D3) radiomarkiert und an postmortalen Hirnschnitten von Alzheimer-Patienten mittels *in vitro* Autoradiographie getestet und gegen Immunohistochemie validiert.

In der zweiten Studie wurde eine auf Blutlevel basierende Normalisierungsstrategie für die Antikörper-basierte TREM2-PET-Bildgebung entwickelt und validiert. Anhand von PET-Scans von TREM2 KO- und WT-Mäusen, denen der Radioligand [⁶⁴Cu]Cu-NODAGA-ATV:4D9 injiziert worden war, wurde die aus den Bildern abgeleitete Blutaktivität aus dem Herzen extrahiert und mithilfe von SPM mit den *ex vivo* Blutwerten korreliert. Dies ermöglichte die Etablierung eines voxelbasierten Normalisierungsansatzes, der die interindividuelle Vergleichbarkeit von TREM2-

PET Signalen verbesserte. Die Validierung erfolgte durch Korrelation der normierten PET-Signale mit den TREM2-Proteinspiegeln in peripheren Organen (Knochenmark, Leber, Milz, Lunge), die mittels MSD-Technologie gemessen wurden. Der Ansatz wurde anschließend an zwei Krankheitsmodellen (Myokardinfarkt und Alzheimer ($APP^{SAA};TfR^{mu/hu}$)) getestet und zeigte seine Nützlichkeit für die Bildgebung von TREM2 nicht nur im Gehirn, sondern auch in peripheren Organen, wodurch sich das Anwendungsspektrum des Radioliganden erweitert.

Die entwickelten Radioliganden wurden mit einer hohen radiochemischen Reinheit ($> 97,3\%$), radiochemischen Ausbeute ($> 67,1\%$) und spezifischen Aktivität ($1,0-1,4 \text{ MBq}/\mu\text{g}$) gewonnen. Die Konjugation der Chelatoren an den ATV:4D9-Antikörper beeinflusste nicht die agonistische Wirksamkeit gegenüber dem TREM2 und die Stabilität des Radioliganden blieb über 48 h erhalten. Die Analyse der PET- und Biodistributionsdaten ergab, dass der 20 h p.i. PET-Zeitpunkt im Sinne des Signal-zu-Rausch Verhältnisses als optimal identifiziert werden konnte. Die ATV-Technologie ermöglichte eine 4,6-fach erhöhte Aufnahme des Radioliganden [^{64}Cu]Cu-NODAGA-ATV:4D9 im Gehirn von hTfR-exprimierenden Mäusen. PET- und Autoradiographiedaten zeigten eine signifikant erhöhte Radioligandenanreicherung in mikrogliareichen Regionen des Cortex und Hippocampus von Alzheimer-Mäusen im Vergleich zu Wildtyp-Kontrollen. Die selektive Anreicherung des Radioliganden in Mikrogliazellen ($94,8\%$) wurde durch scRadiotracing bestätigt. Zudem konnte die zelluläre Aufnahme die Signalerhöhung im Alzheimer-Mausmodell gegenüber dem Wildtyp erklären. Die *in vitro* Autoradiographie an humanem *post-mortem* Hirngewebe von Alzheimerpatienten zeigte eine erhöhte kortikale Bindung des human-spezifischen Radioliganden (Kortex-zu-weißer Substanz-Ratio $2,4 \pm 0,2$; Median \pm SD), die mit der TREM2-Immunhistochemie übereinstimmte (Kortex-zu-weißer Substanz-Ratio $2,4 \pm 0,5$; Median \pm SD).

Die zweite Studie ergab eine signifikante Korrelation zwischen den aus dem PET-Bild extrahierten Blutwerten und den *ex vivo* gewonnenen Blutwerten ($R^2 = 0,9680$, $p < 0,0001$; Lineare Regression). Die bildbasierte Blutnormalisierung erwies sich als deutlich robuster im Detektieren von Signalclustern im TREM2 PET im Vergleich zur klassischen %ID-Normalisierung. Die TREM2-Signale aus dem Gruppenvergleich korrelierten signifikant mit den gemessenen TREM2-Proteinleveln in den Zielorganen ($R^2 = 0,7450$, $p < 0,0003$; Lineare Regression). In Krankheitsmodellen konnten TREM2-positive Makrophagen im Infarktareal des Herzens sowie aktivierte Mikrogliazellen im Alzheimer-Modell nach Blutnormierung zuverlässig detektiert werden und korrelierten mit Signalen der *ex vivo* Autoradiographie (Myokardinfarkt: $R^2 = 0,8584$, $p = 0,0001$; Alzheimer: $R^2 = 0,6902$, $p = 0,0008$; Lineare Regression).

Die Ergebnisse dieser Arbeit zeigen, dass [^{64}Cu]Cu-NODAGA-ATV:4D9 ein vielversprechender Radioligand für die nicht-invasive Bildgebung von TREM2-positiven Mikrogliazellen *in vivo* ist. Die Kombination aus einem spezifischen Antikörper und dem Einsatz der ATV-Technologie ermöglicht eine effiziente Aufnahme im Gehirn und erstmals eine PET-basierte Bildgebung eines Antikörper-basierten Radioliganden des TREM2 jenseits der Blut-Hirn-Schranke. Die quantitative Auswertung von TREM2 PETs wurde durch die neu etablierte Methode zur Blutnormalisierung erheblich gesteigert, indem sie die Detektionsempfindlichkeit erhöhte und die Übereinstimmung mit der tatsächlichen biologischen TREM2-Expression verbesserte.

TREM2 PET bietet somit das Potenzial für eine frühzeitige und spezifische Diagnose bei der Alzheimererkrankung, ein verbessertes Monitoring der Krankheitsprogression sowie die begleitende Evaluation von Therapien, etwa der kürzlich von der Food and Drug Administration und der European Medicines Agency zugelassenen Anti-Amyloid- β -Therapien. Darüber hinaus könnten auch andere Indikationen wie das Glioblastom oder andere chronisch-entzündliche Erkrankungen von TREM2 PET profitieren. Es erfolgte der Beginn der ersten klinischen Anwendungen. Die Resultate der klinischen TREM2-PET-Untersuchungen werden zeitnah erwartet und werden entscheidende Erkenntnisse über das zukünftige Potenzial der molekularen Bildgebungsmethode TREM2 PET liefern.

3. Introduction

It is estimated that someone in the world develops AD approximately every five seconds (1). AD is the best-known and most prevalent form of dementia and represents an enormous global challenge. It accounts for up to two-thirds of all cases of dementia (2, 3). The World Health Organization estimated that, as of 2019, more than 55 million people worldwide were living with dementia (4, 5). Projections indicate that the number of people with dementia could increase to approximately 78 million by 2030 and 139 million by 2050 due to population aging (4, 6). The global cost of dementia poses an enormous economic burden. It was estimated to be around \$1.3 trillion in 2019 and is expected to double by 2050 (4, 7).

The social and medical urgency of AD is significant. The Alzheimer's Association defines AD as "a type of dementia that affects memory, thinking, and behavior" (8). AD is associated with a progressive loss of independence that hinders individuals from performing daily activities, thereby imposing a substantial burden on both the affected individuals and their families (9, 10).

Despite extensive research and economic efforts, a cure remains elusive, and existing pharmacological interventions offer only modest benefits (2). Recently, amyloid-beta ($A\beta$)-targeting monoclonal antibodies, such as donanemab and lecanemab, have shown potential in slowing disease progression by targeting $A\beta$ aggregates (11, 12). Meanwhile, symptomatic therapies, most notably cholinesterase inhibitors (donepezil, galantamine and rivastigmine) and the *N*-methyl-D-aspartate (NMDA) receptor antagonist memantine, may temporarily relieve cognitive symptoms (13-16).

The diagnosis of AD currently relies on a combination of clinical assessment and confirmation based on biomarkers, typically using cerebrospinal fluid or plasma analysis or PET imaging of $A\beta$ and tau protein (17, 18). However, these biomarkers primarily reflect established pathologies and may not capture early disease progression (17).

Emerging evidence underscores the pivotal role of neuroinflammation, and that microglial activation plays a central role in the early stages of disease pathogenesis long before clinical symptoms appear (19, 20). These findings pave the way for novel imaging biomarkers that could enable earlier diagnosis and potentially more effective therapeutic interventions. The underlying hypothesis states that identifying pathological changes early and initiating therapy before irreversible neurodegeneration occurs could lead to disease-modifying effects (21, 22). The need for early detection and personalized therapeutic monitoring highlights the importance of developing novel imaging approaches.

3.1 AD and the Role of Microglia

3.1.1 Neuropathological Hallmarks of AD

Alois Alzheimer first described the cardinal histopathological features of AD over a century ago and these features remain valid today (23). These comprise the accumulation of A β plaques in the extracellular space and the presence of intracellular neurofibrillary tangles, which consist of tau proteins in a hyperphosphorylated state. Moreover, they are accompanied by widespread synaptic dysfunction, neuronal loss, and progressive cognitive decline (memory loss) (24-28).

Although refined over the years, the amyloid cascade hypothesis continues to serve as the central framework for understanding AD pathogenesis. This hypothesis proposes that the aggregation of A β peptides initiates a cascade of pathological events, including tau hyperphosphorylation, neuroinflammation, synaptic degradation, and neuronal death, ultimately leading to dementia (29-31). More recent evidence highlights the role of the innate immune system, particularly the activation of microglia, in amplifying and possibly initiating these processes in the very early stages of the disease (20, 32-34). Studies have demonstrated that the activation of microglial cells emerges with the onset of amyloid deposition in the brain, decades before symptoms of memory loss appear (19, 35).

Importantly, A β deposition is not uniformly distributed across the brain. Instead, it accumulates preferentially in the neocortex and hippocampus, which are regions involved in memory formation and cognitive processing (36-39). The topography has clinical relevance for functional imaging approaches aiming to visualize AD pathology and is reflected in pathological staging systems, such as Braak staging (40) and Thal phases (41).

3.1.2 Role of Microglia in Neurodegeneration

Microglia, which comprise approximately 10% of all brain cells, are the resident immune cells of the CNS (42-44). Under physiological conditions, they are essential for immune surveillance, synaptic pruning and the maintenance of homeostasis. In response to pathogenic stimuli such as aggregated A β , microglia become activated and undergo extensive transcriptional and functional reprogramming (42, 45, 46).

Recent transcriptomic studies have identified a specialized subpopulation of activated microglia in AD. These cells are characterized by the upregulation of genes such as TREM2, ApoE and Clec7a and the downregulation of homeostatic markers such as P2Y12 and Tmem119. Experimental evidence suggests that activated microglia fulfill a neuroprotective function in the early stages of the disease by promoting A β phagocytosis and forming compact barriers around the plaques (45, 47, 48).

However, chronic activation of microglia can have detrimental effects, as it promotes the release of pro-inflammatory cytokines, oxidative stress and synaptic toxicity. The duality of beneficial

and detrimental microglial responses highlights the complexity of their role in neurodegenerative diseases (45, 49, 50).

Activation of microglia is no longer considered a secondary response to protein aggregation, but rather a primary driver of disease progression. Due to the spatial co-localization of activated microglia with A β plaques, particularly in the cortex and hippocampus, there is growing interest in identifying distinct microglial phenotypes as diagnostic markers and therapeutic targets in AD (32, 51, 52).

3.2 TREM2 Biology and Imaging Potential

3.2.1 TREM2 Structure, Signaling and Function

TREM2 is a type I transmembrane receptor of the immunoglobulin superfamily that is primarily expressed on cells of the myeloid lineage. TREM2 is composed of an extracellular immunoglobulin-like domain, a transmembrane region and a short intracellular domain (53, 54).

TREM2 functions by interacting with two adapter proteins: DNAX-activating protein of 12 kDa (DAP12) and DNAX-activating protein 10 (DAP10) (54-56). Upon binding to its ligands, which include phospholipids, sulfatides (and many other unknown compounds (57)), DAP10/12 is phosphorylated, triggering intracellular signaling cascades. These cascades include the activation of the tyrosine kinase SYK (spleen tyrosine kinase, SYK), followed by many pathways, including phosphatidylinositol 3-kinase (PI3K) and extracellular-signal-regulated kinase (ERK). The result of this process is the initiation of phagocytosis, survival and anti-inflammatory responses in myeloid cells (53, 58-61).

An additional aspect of TREM2 is its cleavage by the proteases disintegrin and metalloproteinase domain-containing protein 10 or 17 (ADAM10/17) within the stalk region, generating soluble TREM2 (sTREM2), which is detectable in the cerebrospinal fluid and blood (62-64). Although its exact role is still being investigated (65-69), elevated levels of sTREM2 in the cerebrospinal fluid of individuals with early-stage AD are believed to reflect microglial activation in response to neuronal injury, suggesting that sTREM2 could be a useful fluid biomarker (70-74).

TREM2 is essential for the phenotypic transition of microglia from a homeostatic to a disease-associated state. In the context of AD, TREM2 is involved in the response of microglia to the accumulation of A β and neuronal injury (53). This makes TREM2 a key modulator of immune activity in AD and a promising research target.

3.2.2 TREM2 in CNS and Periphery

In the CNS, TREM2 is expressed almost exclusively by microglia, the resident immune cells of the brain (75, 76). During neurodegenerative processes, such as AD, TREM2 expression is upreg-

ulated and particularly enriched in the vicinity of A β plaques, where it facilitates microglial clustering and the containment of amyloid pathology. As previously mentioned, sTREM2 can be found in the cerebrospinal fluid (42, 53).

In peripheral tissues, TREM2 is expressed on a wide range of myeloid cells, including macrophages, dendritic cells, granulocytes, and tissue-resident macrophages such as Kupffer cells, splenocytes and osteoclasts (77-82). Although its general role in phagocytosis and tissue repair remains consistent, the precise function and ligand specificity of TREM2 can vary between compartments (57).

3.2.3 Relevance as a Biomarker and Potential Target

TREM2 has emerged as an attractive target in AD research due to its robust genetic, spatial and functional associations with disease pathology. A breakthrough occurred in 2013 with the identification of coding variants in TREM2 (83, 84), most notably the R47H mutation (substitution of arginine with histidine at position 47). This mutation impairs ligand binding to the receptor and significantly increases the risk of late-onset AD (85-90). Genetic evidence underscores TREM2's role in disease onset and progression. In contrast, TREM2 overexpression has been shown to have protective effects, such as enhancing A β clearance and modulating microglial activity (91).

The key role of TREM2 to regulate the microglial response to A β and the spatial co-localization of TREM2-positive microglia with amyloid plaques make TREM2 a promising biomarker for *in vivo* molecular imaging. Unlike traditional neuroinflammation markers, such as TSPO, which are expressed by multiple cell types and are subject to genetic variability in binding affinity (92, 93), TREM2 offers a more specific readout of microglial activation. Its selective expression, upregulation in early disease stages, and functional involvement in immune modulation make it a potential target for diagnostic imaging and a possible entry point for therapeutic intervention, while boosting beneficial microglial functions (94, 95).

By visualizing TREM2 expression *in vivo*, it may be possible to monitor disease progression and evaluate therapies designed to modulate microglial response.

3.3 Molecular Imaging of Neuroinflammation

3.3.1 PET Imaging Principles and Applications

PET is a highly sensitive, non-invasive imaging modality that enables the three-dimensional visualization and quantification of biological processes at the molecular level. PET has become an essential tool in many disciplines including oncology, cardiology and also neurology (96).

PET relies on radioligands, which are molecules that selectively bind to biological targets *in vivo* and are labeled with positron-emitting radioisotopes (β^+ decay). Among the most commonly used PET isotopes is fluorine-18 (^{18}F), which has a physical half-life of approximately 110 minutes and favorable imaging characteristics (97).

Following intravenous injection, the radioligand circulates systemically and accumulates in regions where the target of interest is expressed, driven by the affinity and target density.

When the radionuclide undergoes β^+ decay, the emitted positron travels a short distance in the tissue (typically < 2 mm in soft tissue, (98)) before it encounters an electron. The resulting annihilation generates two photons with energies of 511 keV that are emitted nearly simultaneously in opposite directions ($\approx 180^\circ$ apart). These photons are detected as coincident events by a ring of scintillation detectors within the PET scanner. The detection of multiple such events enables the reconstruction of high-resolution three-dimensional images of the spatial distribution of the radioligand within the body. Hybrid systems such as PET/CT (computed tomography, CT) or PET/MRI combine functional and anatomical data with spatial resolutions below 4 mm for modern systems (99). For further technical information on the PET imaging methodology and reconstruction algorithms, please refer to (100).

PET offers unique advantages in brain imaging. It allows for *in vivo* quantification of receptor density, protein aggregation and immune cell activation. Additionally, PET enables longitudinal studies in patients, providing a tool for monitoring disease progression or therapeutic efficacy over time (101).

In AD, PET imaging plays a central role in visualizing hallmark pathologies including A β plaques and tau tangles. Recently, PET has been used to evaluate neuroinflammatory processes, particularly microglial activation and reactive astrogliosis, offering new insights into immune-related mechanisms of AD pathogenesis *in vivo* (102, 103).

3.3.2 State of the Art and Limitations of TSPO Imaging

TSPO, also known as the peripheral benzodiazepine receptor, is the most widely used PET target for imaging neuroinflammation (104). TSPO is expressed in the outer mitochondrial membrane and upregulated during neuroinflammatory responses in activated glial cells, including microglia, astrocytes and infiltrating macrophages (92, 93).

The first and one of the most widely studied TSPO PET radioligand is (*R*)-*N*-([^{11}C]methyl)-*N*-(1-methylpropyl)-1-(2-chlorophenyl)isoquinoline-3-carboxamide ((*R*)-[^{11}C]PK11195). It provided proof-of-concept and high affinity to TSPO, but was limited by poor signal-to-noise ratio, low brain penetration and a short half-life (20 min for carbon-11) (105, 106). Second- and third-generation TSPO radioligands such as *N,N*-diethyl-2-[2-(4-(2-[^{18}F]fluoroethoxy)phenyl)-5,7-dimethylpyrazolo[1,5-*a*]pyrimidin-3-yl]acetamide ([^{18}F]DPA-714), *N*-Acetyl-*N*-(2-[^{11}C]methoxybenzyl)-2-phenoxy-5-pyridinamine ([^{11}C]PBR28) and (4*S*)-*N,N*-diethyl-9-[2-[^{18}F]fluoroethyl]-5-methoxy-2,3,4,9-tetrahydro-1*H*-carbazole-4-carboxamide ([^{18}F]GE-180) have demonstrated improved binding properties in the brain (107-109). However, key limitations remain:

- i) Lack of cellular specificity:
TSPO is not exclusively expressed in microglia, making it difficult to determine the origin of the signal (93).

- ii) Genetic variability:
A single nucleotide polymorphism (rs6971) affects the TSPO ligand affinity, dividing patients into high-, mixed- and low-affinity binders (110, 111).
- iii) Context sensitivity:
TSPO levels increase in response to various stimuli such as neurodegeneration, injury and peripheral inflammation (112).

Despite these limitations, TSPO PET imaging has advanced the understanding of neuroinflammatory processes in AD (113-115). Researchers are now moving toward identifying more selective targets (116).

3.3.3 TREM2 as an Emerging PET Target

TREM2 provides superior cellular specificity compared to TSPO. It is predominantly expressed by microglia in the brain under both physiological and pathological conditions and is not subject to polymorphisms that affect binding affinity. Furthermore, TREM2 upregulation reflects an activation state of microglia that is closely linked to neurodegeneration and neuroinflammation in AD. These features make TREM2 a promising next-generation target for PET imaging of neuroinflammation (70, 117).

Recent advances in radioligand engineering enabled the development of antibody-based PET radioligands that target TREM2. Unlike conventional small-molecule radioligands, antibodies provide exceptional target specificity and a high affinity for extracellular epitopes expressed on cell surfaces (118). However, due to their large molecular size (~ 150 kDa for immunoglobulin G, IgG), full-size antibodies have a limited ability to cross the BBB, with < 0.1% of the injected dosage reaching the brain (119-126), posing a significant challenge for imaging the brain (127, 128).

To overcome this limitation, researchers have designed bispecific antibodies that combine a high affinity moiety for TREM2 with an additional binding moiety that targets the transferrin receptor 1 (TfR1). The TfR1 facilitates receptor-mediated transcytosis across the BBB, allowing for effective delivery of radioligands into the brain tissue (94) (Figure 1).

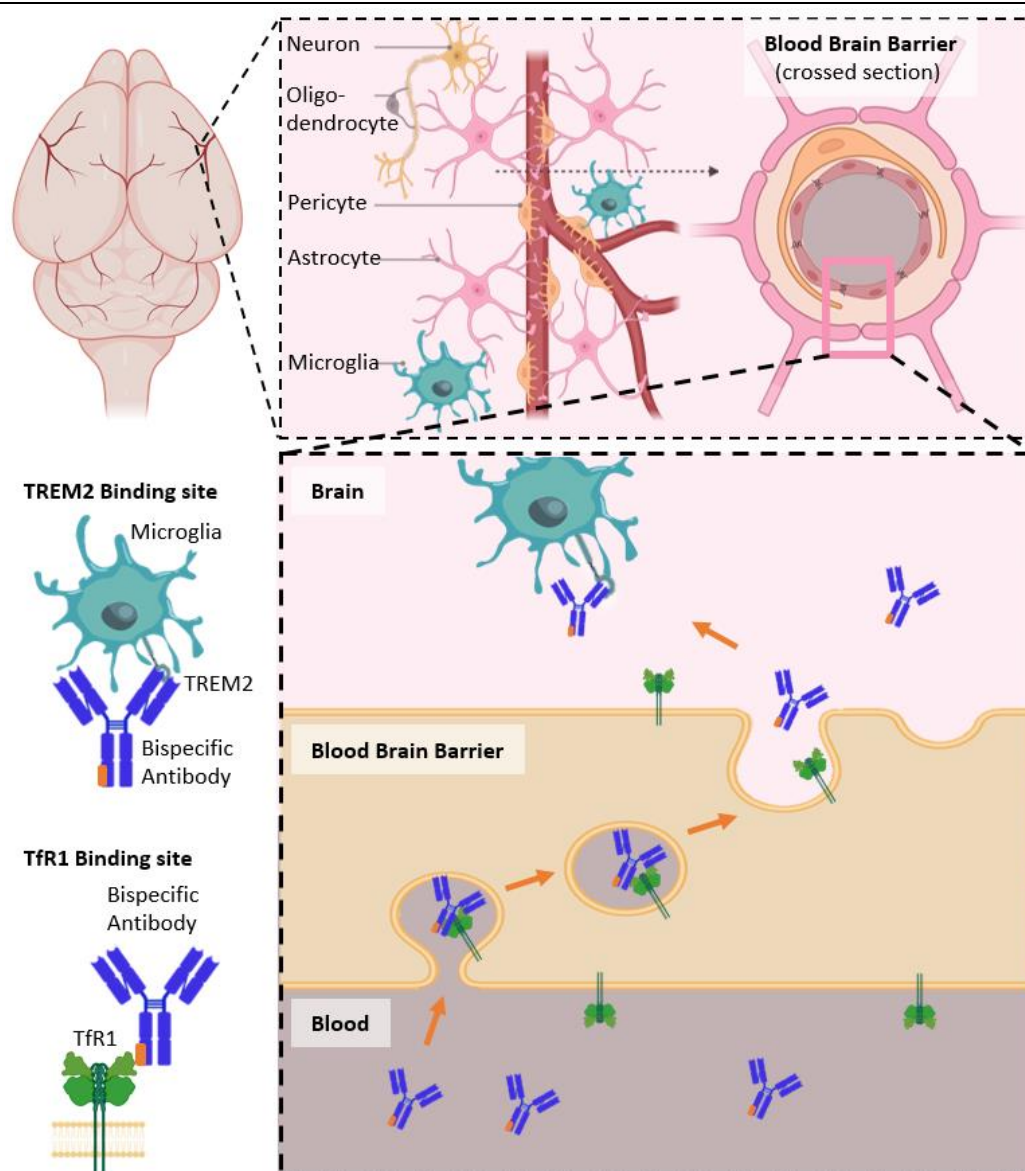


Figure 1. Schematic illustration of a bispecific antibody (anti-TfR1 and anti-TREM2) crossing the BBB.

[¹²⁴I]mAb1729-scFv8D3_{CL}, a bispecific antibody-based radioligand targeting TREM2 and TfR1, was the first TREM2-targeting radioligand tested preclinically *in vivo* in the brain. However, this radioligand failed to demonstrate clear visual and quantitative differentiation between AD and control mice (129). In contrast, the radioligand developed in this study, [⁶⁴Cu]Cu-NODAGA-ATV:4D9, showed a statistically significant accumulation of PET signals in the cortical and hippocampal regions of AD mouse models and enabled distinction between genotypes (130).

This approach represents a novel way of linking innate immune activation to disease progression in AD.

3.4 Considerations for the Development of Antibody-based TREM2 PET Radioligands

3.4.1 Antibody Engineering and BBB Penetration

Antibody-based PET radioligands provide high specificity for extracellular targets (e.g., TREM2); however, their development is challenging, particularly regarding BBB penetration (124, 131, 132).

The use of bispecific antibodies has emerged as a key strategy for overcoming this limitation (see Table 1 for a review of alternative strategies). This involves combining a high-affinity binding domain for a molecular target (e.g., TREM2) with a second specificity that enables receptor-mediated transcytosis. This is most commonly achieved by targeting the TfR1 (133).

Depending on the antibody design, the TfR1-targeting domain can be (I) attached, for example, as a single chain variable fragment (scFv) to the IgG backbone or (II) integrated into the antibody backbone (94).

Table 1. Overview of potential alternative strategies to improve BBB penetration for antibody-based radioligands.

Strategy	Mechanism	Advantages	Limitations	References
TfR1-mediated transcytosis	Receptor mediated transcytosis	Efficient transport	BBB	Requires affinity tuning; risk of peripheral off-targeting (134, 135)
Insulin receptor-targeting shuttles	Receptor mediated transcytosis	Alternative route		Less validated (136, 137)
Antibody fragments (e.g., scFv)	Size reduction	Improved brain access		Rapid clearance; lower stability (138, 139)
Nanoparticles	Encapsulation or conjugation with targeting ligands	Versatility with high payload		Limited CNS targeting specificity; translation challenges (140, 141)
Intranasal delivery	Direct access via olfactory epithelium	Non-invasive; bypasses BBB		Low and variable brain bioavailability (142, 143)

Focused sound	ultra-	Temporarily opens BBB with acoustic waves and microbubbles	Local, transient BBB opening	Requires specialized equipment; uncooperative patients	(144, 145)
----------------------	---------------	--	------------------------------	--	------------

In our studies, we employed a full-length IgG antibody (4D9) that is reactive to mouse TREM2 (146). The antibody was modified by incorporating a TfR1-binding module, called ATV, into the backbone of the antibody. Additionally, the fragment crystallisable region was modified (L234A/L235A) to eliminate effector functions, thereby minimizing immune-mediated cytotoxicity (147).

Notably, the amino acid sequence of TREM2 differs between humans and mice, particularly in the extracellular domain (53). Consequently, the antibody binding and cross-species reactivity must be validated for each construct. Our radioligand targets mouse TREM2 and cannot be directly applied to humans without re-engineering. Furthermore, the antibody construct (ATV:4D9) used in our study binds to an epitope present in both membrane-bound TREM2 and sTREM2 (146). This has implications for radioligand specificity and the interpretation of *in vivo* PET signals.

These strategies demonstrate the technical difficulty of delivering biologics to the CNS and highlight the rationale behind our bispecific receptor-mediated approach. Successful brain uptake of [⁶⁴Cu]Cu-NODAGA-ATV:4D9 in preclinical evaluation confirmed the potential of these constructs for imaging neuroinflammation (130).

3.4.2 Radiolabeling and Chelator Systems

For PET imaging, antibody constructs must be labeled with positron-emitting radionuclides. In the context of PET imaging of neuroinflammation, the relatively slow pharmacokinetics of full-sized antibodies require the use of isotopes with longer half-lives to allow for sufficient target accumulation at a later imaging time-point. Simultaneously, the unbound radioligand should be eliminated from the system at this time (148).

Copper-64 (⁶⁴Cu) ($t_{1/2} = 12.7$ h) is particularly suitable for such applications. It has a favorable half-life and well-established radiochemistry, and can be efficiently incorporated into antibody-based radioligands using chelator systems. Its positron emission properties (β^+ : 17.5% (0.653 MeV)) provide sufficient image quality with slightly lower resolution than that of traditionally used fluorine-18 (149, 150).

Other radionuclides used in antibody-based PET imaging include (151):

- i) Zirconium-89 (^{89}Zr) ($t_{1/2} = 78.4$ h)
It allows for very late time-point imaging but may show accumulation in bones due to the release of free ^{89}Zr *in vivo*, especially if the chelation is suboptimal.
- ii) Iodine-124 (^{124}I) ($t_{1/2} = 100.2$ h)
However, it is prone to *in vivo* dehalogenation, which limits its use.
- iii) Gallium-68 (^{68}Ga) ($t_{1/2} = 68$ min)
It is commonly used for imaging peptides and small-molecules but is less compatible with full-sized antibodies for brain imaging because of its shorter half-life and lower image quality.

Radiometals such as copper-64 cannot be directly attached to antibodies, so bifunctional chelators are used instead (152). These chelators must match the ionic radius, oxidation state and coordination chemistry of the selected radionuclide (153). In our studies we used *p*-NCS-benzyl-NODAGA, a macrocyclic chelator with strong affinity for Cu(II). The isothiocyanate group of *p*-NCS-benzyl-NODAGA reacts with the primary amine groups (lysine residues) that are located on the antibody surface, forming stable thiourea bonds. This conjugation strategy offers excellent *in vivo* stability and labeling efficiency under mild conditions. However, this conjugation strategy is non-specific because of the abundance of lysine residues (154, 155).

Conjugation of the chelator to the antibody should be site-specific to preserve the antigen-binding affinity and pharmacokinetics. Modern conjugation strategies include maleimide-thiol chemistry (e.g., via engineered cysteines), enzymatic methods and click chemistry. These approaches allow for consistent chelator-to-antibody ratios and reduced variability in biodistribution and clearance (156, 157).

3.4.3 Preclinical Imaging in AD Mouse Models

Mice (*Mus musculus*) do not develop AD naturally. Nevertheless, mouse models of AD are indispensable in AD research and have been developed with great effort to better understand the pathophysiology of AD and evaluate therapeutic strategies (158, 159). The mice are generated as transgenic mouse models by overexpressing human genes carrying mutations associated with autosomal dominant Familial Alzheimer's disease (FAD, (160)) that accelerate disease progression. These mutations are randomly integrated into the mouse genome and include the substrate beta-amyloid precursor protein (APP, (161, 162)) gene, the proteases presenilin 1 (PSEN1, (163)), and the presenilin 2 (PSEN2, (164)) gene, all of which play central roles in A β (165) plaque formation.

The transmembrane glycoprotein APP is cleaved by proteolytic secretases, which leads to the formation of A β . The presenilin encodes the catalytic subunit of the γ -secretase complex responsible for the cleavage (166).

More recent generations include knock-in (KI, (167)) and knock-out (KO, (168)) mice, which are often generated using Clustered Regularly Interspaced Short Palindromic Repeats (CRISPR, (169)) gene editing technology to accurately represent human AD pathologies and avoid the over-expression of human AD genes. Mouse models vary widely in the extent to which they exhibit AD-relevant features, including A β and tau accumulation, glial activation, neurodegeneration, and cognitive or behavioral impairments (159, 170).

No mouse model fully reproduces the complexity of sporadic AD in humans, which remains a major limitation for translational research (170-172). However, multigenetic mouse models combining A β , tau and neuroinflammation are being developed to address this gap (173-176).

In our studies, we employed two complementary amyloidosis models: B6.Cg-Tg(APP^{Sw}-F1Lon,PSEN1*^{M146L}*^{L286V})6799Vas/Mmjax (hereafter 5xFAD), and *APP^{SAA}*.

One of the most widely used amyloidosis models is the transgenic 5xFAD mouse line (159). These mice express human APP and PSEN1 with five FAD mutations: The Swedish mutation (APP, KM670/671NL), which increases total A β production via enhanced cleavage of the APP via the β -secretase; the Florida (APP, I716V) and London (APP, V717I) mutations, both increasing the A β ₄₂/A β ₄₀ ratio; and PSEN1 mutations M146L and L286V, which further promote A β ₄₂ production (177, 178). In hemizygous animals, amyloid plaques appear in the cortex and hippocampus as early as 2-4 months of age (177), with female mice showing a more severe pathology than males (179, 180). Microgliosis begins at around four months and is spatially associated with A β plaques (179).

The *APP^{SAA}* KI line incorporates a humanized A β sequence into the endogenous mouse APP gene with three AD-related mutations: the Swedish mutation (KM670/671NL), which enhances total A β levels; the Arctic mutation (E693G), which accelerates A β protofibril formation; and the Austrian mutation (T714I), which increases the A β ₄₂/A β ₄₀ ratio. From four months of age, homozygous *APP^{SAA}* mice develop progressive amyloid plaque accumulation, cerebral amyloid angiopathy, and are associated with microgliosis and dystrophic neurites. Importantly, the gene expression profiles of phagocytic plaque-associated microglia in this model significantly overlap with those observed in the human AD brain. TREM2 expression levels are also elevated in brain lysates of *APP^{SAA}* mice (181).

We used both of these mouse models in our studies, all well as versions with an additional KI of the hTfR gene to enable brain uptake of TfR1-targeting radioligands.

In addition to amyloidosis models, TREM2 KO mice were used in the second study to validate radioligand specificity and investigate improved PET quantification strategies. These mice lack TREM2 expression and were compared with wild-type controls in the context of image-derived blood normalization. Their inclusion was essential for demonstrating the biological relevance of PET signal differences.

All lines were bred on a WT background, which served as the wild-type control to account for non-AD-related effects.

3.4.4 Outlook on Clinical Translation

The translation of PET radioligands from preclinical to clinical applications involves technical, regulatory and biological considerations. In the case of TREM2 imaging, it requires careful adaptation of radioligand production and quality control is required to comply with Good Manufacturing Practice standards (182).

While preclinical studies rely on high-expression models and small-animal PET scanners with high nominal spatial resolution (~ 1 mm), the relative resolution of clinical PET (~ 4-5 mm) is comparable or even favourable when scaled to the human brain (99, 183-187). In fact, with successful BBB penetration and adequate target engagement, the larger brain volume in patients may even allow for improved signal distribution and reduced spill-over from surrounding structures, such as the skull.

Nevertheless, TREM2 expression levels in the human brain are generally lower and more heterogeneous between AD patients vs. non-AD controls than in AD mouse models and respective mouse controls (188, 189). Additionally, injected activity in humans remains significantly lower relative to body weight than in animal studies (190, 191). This may affect the signal intensity and contrast, requiring optimized acquisition protocols and robust image processing strategies to enable reliable quantification and interpretation of clinical TREM2 PET scans.

The first clinical applications have been initiated in patients. Although these studies are beyond the scope of this dissertation, they are an important translational step that will contribute to understanding the diagnostic value of TREM2 PET.

3.5 Improved Quantification Strategies for TREM2 PET

3.5.1 Challenges in Quantifying Antibody-Based Radioligands

The quantification of antibody-based PET signals in the brain presents specific challenges, primarily due to the slow pharmacokinetics of these large biomolecules and the late imaging time-points, which are typically required to achieve adequate tissue contrast. Unlike small-molecule radioligands, IgG antibodies demonstrate delayed tissue penetration and prolonged circulation time. Consequently, imaging is often performed 24 hours after injection to allow for sufficient radioligand accumulation in the target tissue and clearance from the blood (124, 131).

These characteristics complicate the use of standard metrics, such as %ID- or standardized uptake value-(SUV)-normalization, which assume a relatively stable distribution of radioligands at the time of imaging (192-194). For TREM2 PET in particular, the slow accumulation of radioligands in brain regions with low target expression can lead to a high background signal from circulating radioligands. This reduces image contrast and can mask subtle but biological meaningful differences in TREM2 expression.

Additionally, antibody uptake in the brain is generally low and target expression in neuroinflammatory conditions such as AD is relatively diffuse, unlike the focal expression patterns observed in brain tumors, for example. These factors require tailored quantification strategies that consider systemic radioligand availability and variability between subjects.

One conceptual consideration comes from the well-established “free drug hypothesis”: Only the unbound fraction of a drug in plasma is available to interact with its target (195, 196). Therefore, blood levels must be carefully considered when interpreting tissue uptake, especially at late imaging time-points, when distribution and clearance kinetics vary significantly across subjects or genotypes.

3.5.2 %ID Normalization vs. Blood-Based Approaches

The aim of quantitative PET imaging is to derive biological information from the distribution of radioligands in the tissues *in vivo*. This can be particularly challenging for antibody-based radioligands due to their slow blood clearance, low brain penetration and variable target expression.

A variety of semiquantitative approaches exist. They include:

Injected dose normalization (%ID or SUV)

Static metrics, such as %ID (measured as the percentage of decay-corrected injected activity per gram (or cubic centimeter) of tissue (%ID/g)) and SUV, are commonly used in PET quantification. They normalize tissue activity to the injected dose (and optionally to body weight in the case of SUV) under the assumption that radioligand distribution has reached a relatively stable equilibrium and is homogeneously distributed throughout the body (192).

$$\% \frac{ID}{g} = \frac{\text{measured radioactivity per gram tissue} \left[\frac{Bq}{g} \right]}{\text{total injected radioactivity} [Bq]} \times 100$$

$$SUV = \frac{\text{measured radioactivity per gram tissue} \left[\frac{Bq}{g} \right] \times \text{animal weight} [g]}{\text{total injected radioactivity} [Bq]}$$

However, this assumption is often inaccurate for antibody-based imaging. Due to the slow clearance of antibodies from the blood and their prolonged circulation, a substantial portion of the radioligand may still be in the vascular compartment at the time of imaging, resulting in the overestimation of tissue uptake. Moreover, residual activity at the injection site can lead to overestimation of the injected dose, further compromising quantification accuracy (197, 198).

Blood level normalization

In contrast, blood level normalization, such as dividing tissue uptake by blood activity, offers a semiquantitative correction for systemic ligand availability.

$$\% \frac{\text{Blood level}}{g} = \frac{\text{measured radioactivity per gram tissue}}{\text{measured radioactivity per gram blood}} \times 100$$

Importantly, blood-based normalization uses blood activity (caution, in the case of PET imaging whole blood levels, not plasma levels) measured at the time of imaging, accounting for the radioligand's current pharmacokinetic state. This is particularly relevant for antibody-based radioligands, where imaging is often performed at delayed time-points (e.g., ≥ 24 h p.i.) when the systemic distribution may still be changing.

Although not an ideal substitute for full kinetic modeling (199), it more accurately reflects physiologically meaningful ligand availability at the time of measurement than SUV or %ID alone.

Blood normalization has been used in both preclinical and clinical studies, particularly in the context of dynamic PET scans. In these cases, an image-derived input function is often used, where vascular structures with high radioligand signals and minimal partial volume effects (e.g., the left ventricle, ascending aorta, carotid arteries or femoral arteries) are segmented directly. This non-invasive estimation of blood activity over time can then be used to normalize tissue uptake or serve as an input for kinetic modelling (200-204).

In our follow-up study, we demonstrated that normalizing TREM2 PET images to blood radioactivity levels is essential for comparing groups with different levels of target expression. For example, it was necessary when comparing WT vs. TREM2 KO mice.

3.6 Aims

The aim of this study was to develop and validate the first microglia-specific TREM2-targeting PET radioligand with an integrated brain shuttle system, enabling the imaging of activated microglia in AD using PET. Mouse models of AD and control mice were included to test both the TREM2-targeting approach for imaging AD pathology via PET and the utility of the integrated brain shuttle system. Additionally, *in vitro* autoradiography was conducted as a pilot study for translation into human imaging.

Furthermore, the quantitative analysis of TREM2 PET imaging was optimized. Methodologically, blood normalization was compared to the standard %ID normalization and validated in mouse models of AD and myocardial infarction.

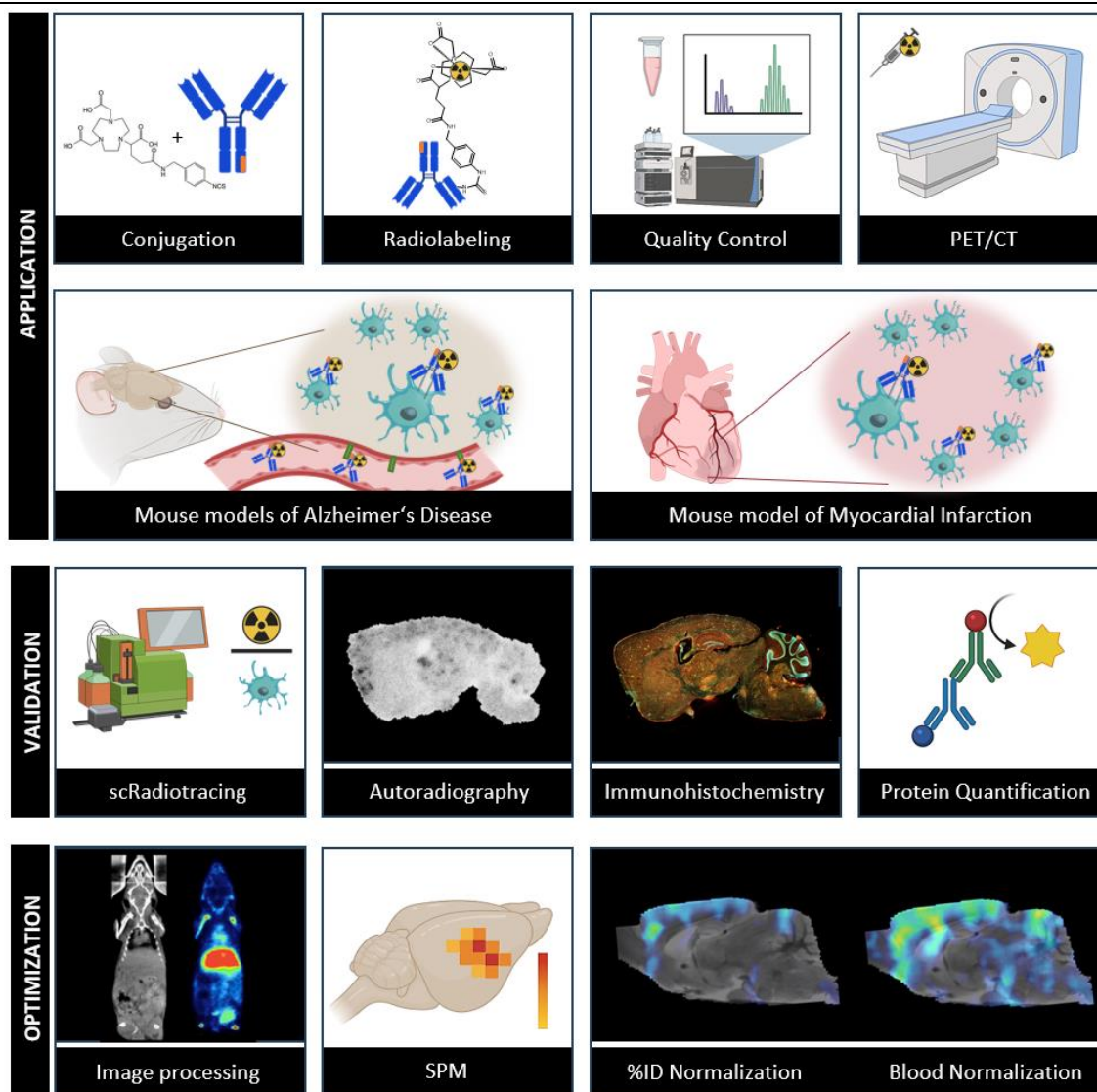


Figure 2. Graphical Abstract of the doctoral thesis. A visual representation of the application, validation and optimization of the TREM2 PET methodology. Created with BioRender.com.

4. Content of the Doctoral Thesis

In this chapter, the most important results are outlined, followed by a concise discussion of the results. Each publication was assigned a sub-chapter. A methodological explanation is provided in the "Method Box" for any method that the author primarily employed during her studies.

4.1 Targeting Microglia in AD: A PET Imaging Approach with Copper-64 labeled TREM2 Antibodies

The study (130) presented in the first paper investigated the hypothesis that a TREM2-targeting radioligand could be an effective tool for visualizing activated microglia involved in neuroinflammation associated with AD pathology. A radioligand based on a TREM2-targeting antibody with and without an integrated brain shuttle system (known as ATV, (147)) was developed and preclinically evaluated in a mouse model of AD (5xFAD, (179)). This study also tested the hypothesis that a brain shuttle system is essential for PET imaging to deliver sufficient antibody-based radioligands to the brain. Furthermore, the specific binding of radioligands to microglial cells at the cellular level was investigated. Finally, the potential for translating this approach to human PET imaging was explored in a pilot project using human brain tissue from AD patients and validated by *in vitro* autoradiography and immunohistochemistry.

Radioligand Design and Validation

TREM2-targeting antibodies with (ATV:4D9, (205)) and without the brain shuttle (4D9, (146)) were conjugated with the chelator *p*-NCS-benzyl-NODAGA (conditions: 7 μ mol chelator, 27 nmol antibody, 0.1 M sodium phosphate buffer, pH 8.5, 4 °C, overnight) to form NODAGA-ATV:4D9 and NODAGA-4D9. These were radiolabeled with copper-64, a positron-emitting radionuclide ($T_{1/2}$ = 12.7 h, 17.5% β^+ emission) well suited for antibody-based PET imaging (206-208). Following conjugation, an spectroscopy-based arsenazo assay (209) confirmed an average of 1-2 chelators per antibody. A low number of chelators per antibody is optimal to preserve immunoreactivity and avoid changes in biodistribution (156). A p-SYK phosphorylation assay (146) using HEK293 Flp-In cells stably expressing mouse TREM2 verified that antibody binding was not compromised by chelator conjugation, which could potentially accrue because chelator conjugation is region-unselective and could bind to the antibody epitope, impairing the antibody binding site. SDS-PAGE (sodium dodecyl sulfate-polyacrylamide gel electrophoresis, (210)) confirmed antibody integrity after modification.

Radiolabeling with [^{64}Cu]CuCl₂ (conditions: 100-200 μ g antibody, 100-200 MBq, 0.1 M ammonium acetate buffer, pH 5.6, 30 min) yielded [^{64}Cu]Cu-NODAGA-ATV:4D9 and [^{64}Cu]Cu-NODAGA-4D9 with a radiochemical yield of 67.1%, purity of 97.3% and specific activity of 1.0 ± 0.2 MBq/ μ g. High-performance liquid chromatography (211) and SDS-PAGE confirmed the intact size of the radioligands.

[^{64}Cu]Cu-NODAGA-ATV:4D9 remained stable after incubation in murine plasma at 37 °C for 48 h, and *ex vivo* analysis 20 h p.i. confirmed the molecular integrity and absence of free copper-64 (*via* radio-thin-layer-chromatography).

In Vitro Autoradiography Results

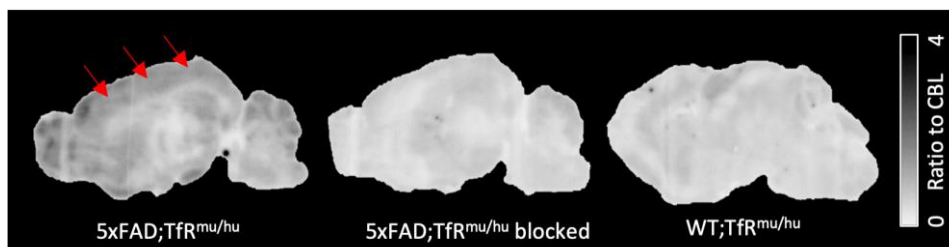


Figure 3. *In vitro* autoradiography of a representative AD mouse brain (5xFAD;TfR^{mu/hu}) vs. a blocked control and pathology-free WT control. Red arrows highlight the cortex. Adapted from (130), licensed under CC BY 4.0.

Following radioligand modification and radiolabeling, *in vitro* autoradiography was conducted on brain slices from 5xFAD;TfR^{mu/hu} mice (n = 4), which express AD pathology, and WT;TfR^{mu/hu} mice (n = 3) as a control to test the potential of the radioligand [^{64}Cu]Cu-NODAGA-ATV:4D9 in terms of functionality and specificity. A 1000-fold molar excess of non-radioactive ATV:4D9 was used as a negative control, a strategy known as self-blocking. *In vitro* autoradiography is conceptually similar to direct immunohistochemistry. Perfused brain slices are incubated with the radioligand, and the distribution patterns of the radioactive substances are visualized by capturing decay emissions on a phosphor imaging plate, which is subsequently read out using a laser scanner (212, 213). The autoradiography revealed specific binding of the radioligand in the cortex and hippocampus of 5xFAD;TfR^{mu/hu} mice, co-localizing with the topography of activated microglia in this mouse model (214-217) (Figure 3). Blocked sections and WT;TfR^{mu/hu} controls showed minimal radioactivity signals, confirming the specificity of radioligand binding. Quantitative analysis of the cortex-to-cerebellum ratio revealed a 1.7-fold higher uptake in 5xFAD;TfR^{mu/hu} mice compared to WT;TfR^{mu/hu} mice.

In Vivo PET Imaging and Biodistribution

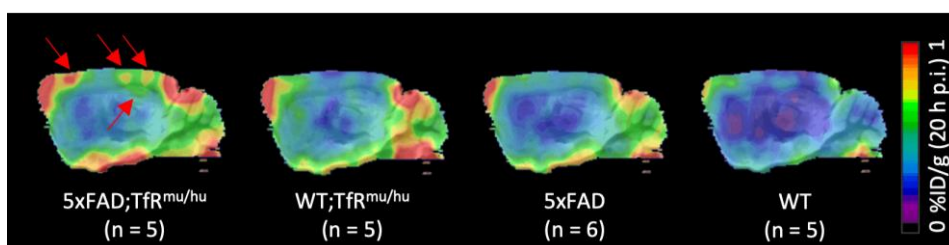


Figure 4. Average TREM2 PET images 20 h p.i. of AD mouse brains vs. WT controls harboring the hTfR for the brain shuttle system (5xFAD;TfR^{mu/hu} and WT;TfR^{mu/hu}) and without the brain shuttle (5xFAD and WT). Red arrows indicate the cortex and hippocampus. Adapted from (130), licensed under CC BY 4.0.

Encouraged by the promising *in vitro* results, we proceeded with *in vivo* PET/CT imaging to assess the radioligand distribution in mice. Four groups of mice were used: the 5xFAD;TfR^{mu/hu} AD model and WT;TfR^{mu/hu} as a control with the working brain shuttle system using [⁶⁴Cu]Cu-NODAGA-ATV:4D9, and the corresponding 5xFAD and WT mice without the working brain shuttle system using [⁶⁴Cu]Cu-NODAGA-4D9 as radioligand. TREM2 PET/CT scans were conducted at three time-points: Early (2 h p.i.), medium (20 h p.i.), and late (40 h p.i.) to identify the optimal imaging time-point.

Our analysis revealed that the best imaging time-point for detecting significant differences in the brain between the groups, in terms of signal-to-noise ratio, was 20 h p.i. At this time, we observed enhanced signal differences in the hippocampus, which is a small and challenging brain region for imaging, compared to the frontal cortex (Figure 4). These findings are consistent with those of previous studies in literature, suggesting that antibody-based PET imaging benefits from later imaging time-points due to prolonged circulation times (218-220). Notably, the 40 h p.i. time-point was excluded due to limited signal-to-noise ratios. A comprehensive overview of the PET image processing workflow is provided in Method Box 1 (Figure 5).

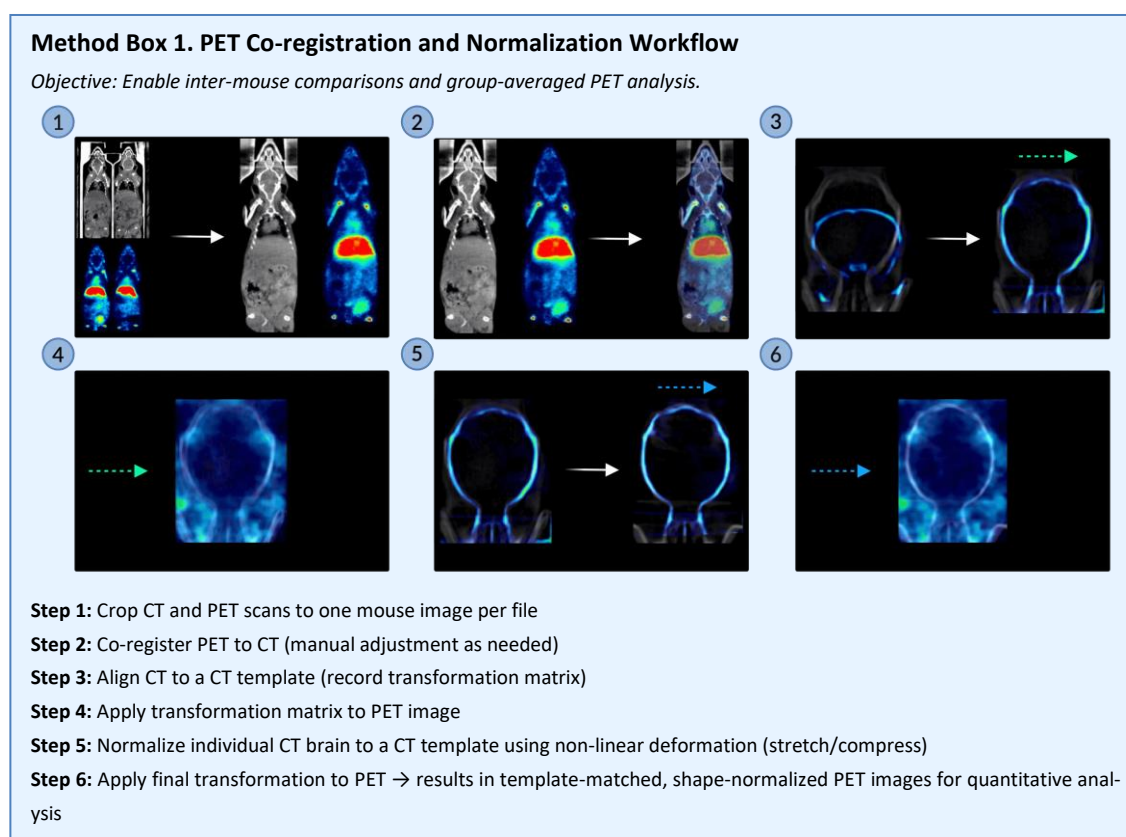


Figure 5. Method Box 1. PET image processing workflow.

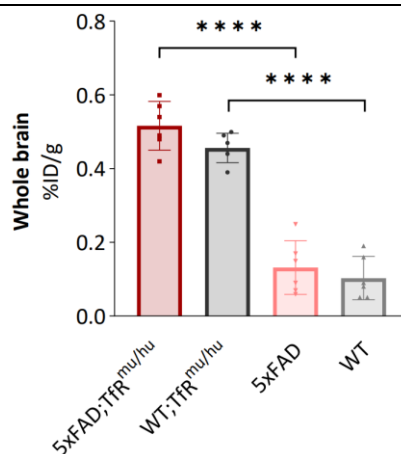


Figure 6. Radioligand uptake in perfused brains at 20 h p.i. One-way ANOVA/Tukey's multiple comparison test, $p < 0.01$ (**). Adapted from (130), licensed under CC BY 4.0.

After TREM2 PET, the brains were collected after perfusion to remove radioactive signals from the blood (clear images of radioligand levels from the blood). The hTfR-mediated transcytosis facilitated significantly higher brain uptake of the radioligands in mice with the working brain shuttle system (Figure 6). At 20 h p.i., 5xFAD;TfR^{mu/hu} mice showed a 4.6-fold higher brain uptake compared to 5xFAD mice, while WT;TfR^{mu/hu} mice exhibited a 4.4-fold higher uptake compared to their counterparts without the brain shuttle system. This confirms that the TfR1-mediated transport system plays a key role in facilitating the delivery of radioligands into the brain (147, 205), enhancing the imaging signal in both AD and wild-type mice.

A comparison of the radioligand concentrations in the brains of the subjects in our study with data reported in the literature for bispecific radioligands targeting either TREM2 or A β and the TfR1 revealed higher brain concentrations in our study (124, 129). However, even higher concentrations in the brain were observed when using a smaller TfR1-targeting bispecific tribody construct (over 1 %ID/g, (221)), which is matching the uptake seen with low-molecular-weight radioligands.

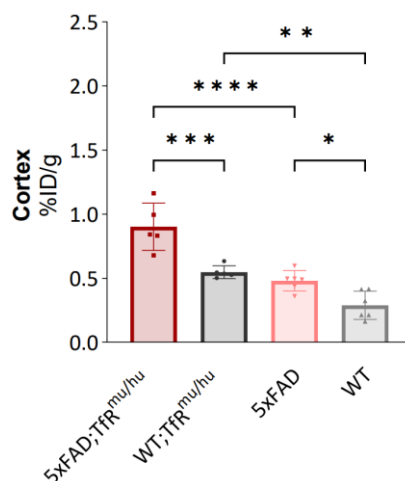


Figure 7. Radioligand uptake in the cortex of the brain 20 h p.i. after perfusion. One-way ANOVA/Tukey's multiple comparison test, $p < 0.01$ (**). Adapted from (130), licensed under CC BY 4.0.

We observed a significantly increased radioligand uptake in the frontal cortex (and hippocampus), where pathology of AD is high (214, 215), at 20 h p.i. in AD vs. WT control mice (%ID/g: 5xFAD;TfR^{mu/hu} 0.902, WT;TfR^{mu/hu} 0.548, 5xFAD 0.480, WT 0.289, $n = 5-6$ per group), demonstrating that the radioligand is capable of revealing TREM2-related signal enhancement (Figure 7). We benchmarked the cortical signal difference of [⁶⁴Cu]Cu-NODAGA-ATV:4D9 in TREM2 PET between 5xFAD;TfR^{mu/hu} and WT;TfR^{mu/hu} to different TSPO-targeting radioligands and found higher %ID/g (1.64 vs. 1.22-1.38, (222-225)) and SUV (1.45 vs. 1.07-1.42, (117, 226-229)) ratios for our TREM2-targeting radioligand.

Role of TfR1 Binding in Brain Uptake

Next, we explored how much of this brain uptake is attributed to TfR1 binding vs. TREM2 binding, since we have a bispecific radioligand in the case of [⁶⁴Cu]Cu-NODAGA-ATV:4D9. We conducted an experiment on the brain uptake in WT;TfR^{mu/hu} mice ($n = 5$ per group) with low TREM2 expression with the radioligand [⁶⁴Cu]Cu-NODAGA-ATV:ISO (an isotype control that binds only TfR1) at 20 h p.i. and compared it to the brain uptake of [⁶⁴Cu]Cu-NODAGA-ATV:4D9 (both TfR1 binding and TREM2 binding) and found that 80% of the total brain uptake was due to TfR1 binding. Since there was the same amount of TfR1 expression in 5xFAD;TfR^{mu/hu} and WT;TfR^{mu/hu} mice (205), we concluded that the significant signal enhancement in the cortex of 5xFAD;TfR^{mu/hu} mice was due to TREM2 expression.

Moreover, no statistical difference between genotypes in whole brain radioactivity level measurements seems reasonable in comparison, as PET allows regional assessment of radioligand uptake.

It should also be noted that the fraction of cortical TREM2 signal in 5xFAD;TfR^{mu/hu} and 5xFAD mice remained constant. The brain shuttle system is responsible for higher radioligand uptake but does not account for a larger relative fraction of TREM2 binding.

The regional TREM2 PET sensitivity is likely to increase in clinical applications because of the higher resolution relative to brain size and the reduced effect of adjacent spill-overs from the skull into the brain.

Ex Vitro Autoradiography Results

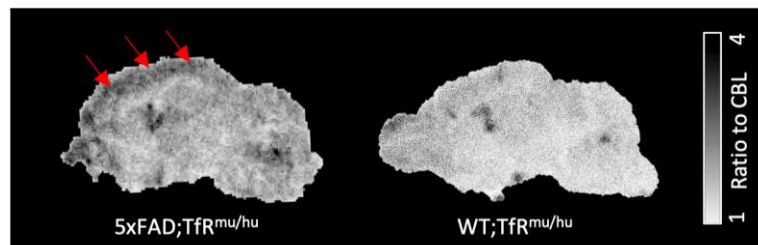


Figure 8. *Ex vivo* autoradiography of a representative AD mouse brain (5x FAD; TfR^{mu/hu}) vs. WT control, 20 h p.i. and after perfusion. Red arrows mark the cortex. Adapted from (130), licensed under CC BY 4.0.

Ex vivo autoradiography 20 h p.i. confirmed regional radioligand distribution in brain slices from 5x FAD; TfR^{mu/hu} and WT; TfR^{mu/hu} mice (n = 2 each, different regions analyzed), further validating the cortical enrichment of TREM2 signals (Figure 8). For *ex vivo* autoradiography, (perfused) brains are sliced into approximately 20 μ m thick slices and the biodistribution of a radioactive substance is shown on a phosphor storage plate generated by the pattern of decay emissions (212, 213).

Cell-Type Specificity via scRadiotracing

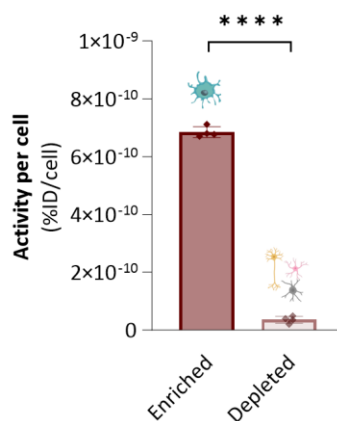


Figure 9. Radioactivity measurements per single cell in the microglia (cluster of differentiation 11b, CD11b) enriched and depleted fractions. (Microglia blue, neurons yellow, astrocytes pink, oligodendrocytes gray). Adapted from (130), licensed under CC BY 4.0. Created with BioRender.com.

Next, we aimed to examine the specificity of the radioligand [⁶⁴Cu]Cu-NODAGA-ATV:4D9 for microglia cells by conducting scRadiotracing (230, 231), a method that allows to determine the radioactivity per single cell, on aged *APP^{SAA}; TfR^{mu/hu}* mice (n = 4, 20 \pm 1 month, high TREM2 levels (181)). scRadiotracing confirmed the high selectivity of the radioligand for microglial cells against non-microglial cells (6.9×10^{-10} vs. 3.6×10^{-11} %ID/cell) (Figure 9, see Figure 10 for the methodology).

It is important to note that CD11b, which is a surface protein on microglial cells (232), was used as a general microglial marker. This limits direct conclusions about TREM2-specific binding at the cellular level.

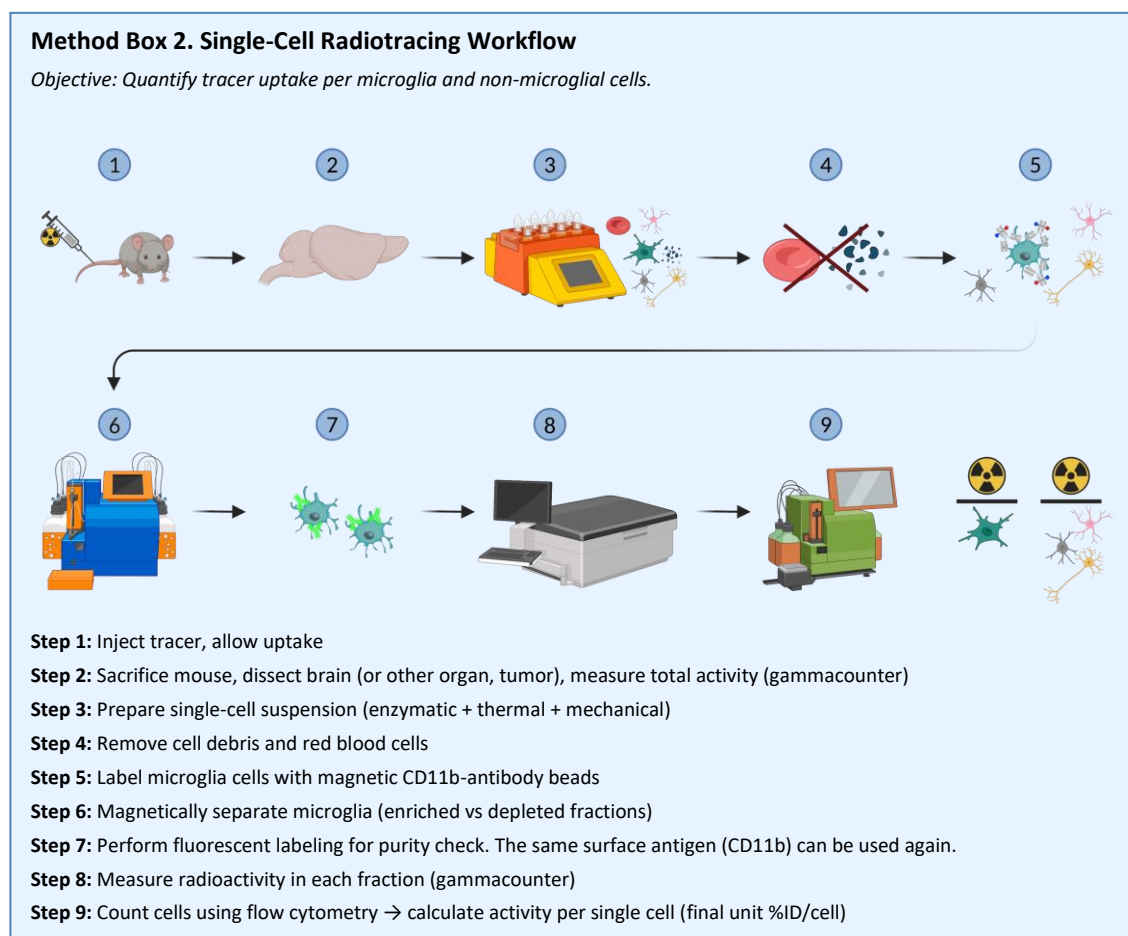


Figure 10. Method Box 2. Workflow of scRadiotracing. Created with BioRender.com.

Translational Application in Human AD Tissue

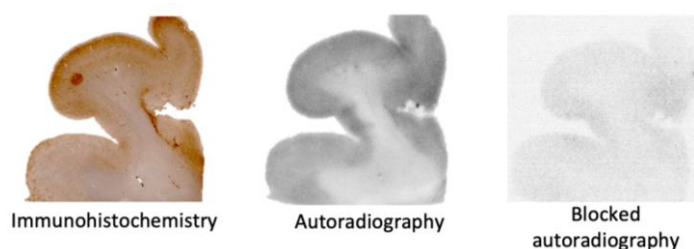


Figure 11. Representative TREM2 immunohistochemistry and *in vitro* autoradiography as well as blocked *in vitro* autoradiography of a human brain section from an AD patient. Adapted from (130), licensed under CC BY 4.0.

Finally, we conducted a pilot experiment for translation into clinical imaging. We radiolabeled a human-specific TREM2 antibody (14D3, (233)) and performed *in vitro* autoradiography and immunohistochemistry (TREM2, A-beta, tau protein) on *post-mortem* brain tissue sections from AD

patients (n = 6). TREM2 immunohistochemistry and autoradiography of the brain sections revealed co-localization, particularly in cortical regions, while subcortical white matter exhibited minimal to no radioligand accumulation (Figure 11). Our results confirmed a spatial correlation between increased TREM2 expression and the presence of AD-related hallmarks, including A β deposits and tau pathology. This aligns with the findings in literature that TREM2-positive microglia cluster around amyloid plaques in both mice and patients (234, 235). Immunohistochemistry and autoradiography yielded comparable cortex-to-white matter ratios (median \pm SD 2.4 ± 0.5 and 2.4 ± 0.2 , respectively), thereby supporting the reliability of both approaches for detecting TREM2. Blocking experiments using the non-radioactive 14D3 antibody at a molar ratio of 1000:1 relative to the radioligand resulted in minimal residual signal, indicating low levels of non-specific binding in the autoradiography assay.

In the context of my shared first authorship "*PET imaging of microglia in Alzheimer's disease using copper-64 labeled TREM2 antibodies*" (130), the results were published in *Theranostics* in September 2024.

4.2 Enhancing Quantitative Analysis of TREM2 PET Imaging: Image-Derived Blood Normalization in Mouse Models

This follow-up study, published in the second paper (236), built upon the findings of the initial study and tested the hypothesis that normalizing PET images to radioligand levels in the blood provides a more accurate quantitative representation of TREM2-specific signals than the standard normalization of the %ID. This is of high interest, as current research highlights TREM2 as a molecular target of interest for both diagnostic imaging and therapeutic intervention (129, 237-239). First, we examined whether image-derived radioactivity values of the blood, which were segmented from PET scans, could be substituted for manually sampled blood values. We then investigated the hypothesis that blood-normalized PET images would better reflect biological TREM2 biodistribution than %ID normalization. To test this hypothesis, we compared the differences in TREM2 signal between WT and TREM2 KO mice (240) to TREM2 protein expression in peripheral organs. Finally, we validated and confirmed the superiority of the blood normalization approach for enhanced quantitative TREM2 analysis in two disease models: AD (*APP^{SAA};TfR^{mu/hu}*) and myocardial infarction, employing SPM, *ex vivo* autoradiography and immunohistochemistry.

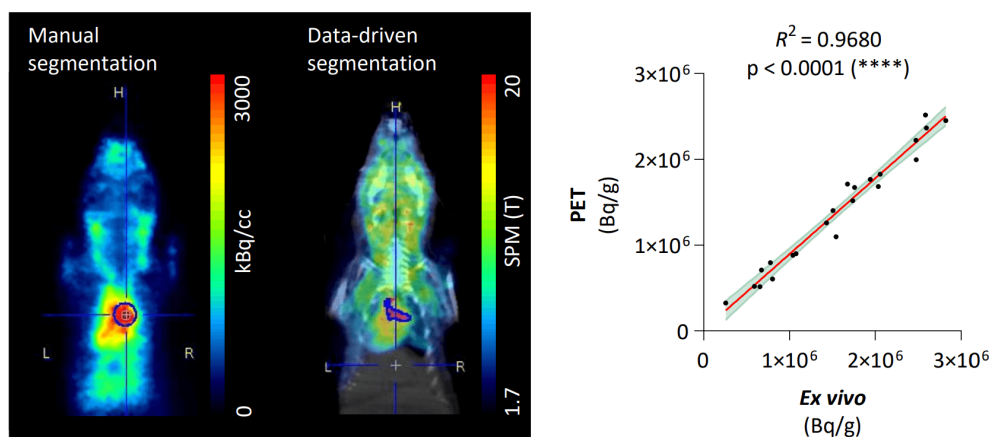


Figure 12. The figure illustrates the volumes-of-interest (VOIs) utilized for blood segmentation from the heart. Manual segmentation of PET images using a spherical VOI. SPM-derived VOI employed in a data-driven approach to segment radioactivity levels from the blood. A significant correlation between blood samples of WT and TREM2 KO mice ($n = 11$ each) obtained *ex vivo* following PET imaging and the segmented blood radioactivity levels derived from PET utilizing a data-driven approach. Linear regression, 95% confidence interval. Adapted from (236), licensed under CC BY 4.0.

First, we investigated whether PET image-derived blood radioactivity levels could be substituted for measurements of manually drawn blood samples. This approach would have several advantages, including a reduction in workload and the ability to perform image analysis with blood normalization of PET images, even in cases where blood samples were not obtained. Therefore, we segmented the blood levels from TREM2 PET scans of WT and TREM2 KO mice ($n = 11$ per group) with [⁶⁴Cu]Cu-NODAGA-ATV:4D9 20 h p.i. In a first approach, we used a manually placed sphere ($r = 2$ mm) in the blood pool of the heart (Figure 12). In the second approach, a data-driven approach using SPM (SPM12 in MATLAB (v2011-R2016), (241)) was employed to find a region in which PET signal intensity significantly correlated with *ex vivo* blood levels (the SPM workflow is summarized in Figure 13). This data-driven volume-of-interest (VOI) (12.1 mm³) was also located in the cardiac blood pool (Figure 12). Both methods demonstrated a significant correlation with the actual blood measurements (manual $R^2 = 0.9492$, data-driven $R^2 = 0.9680$, linear regression). A slight underestimation of data-driven blood levels can be attributed to special alignment variability across animals.

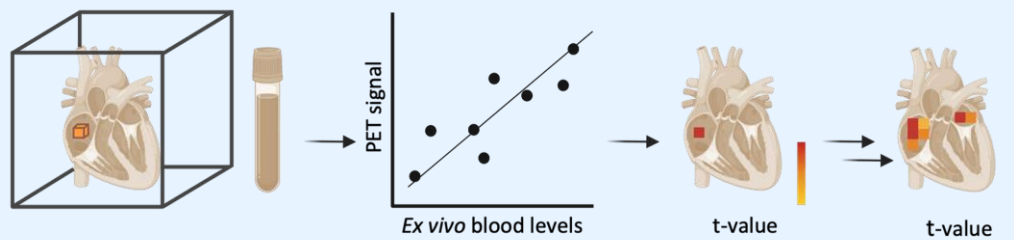
To assess a potential bias between the measurement methods, a Bland-Altman analysis (242) was conducted, which revealed a more systematic offset and reduced variability in the data-driven method (bias 171 kBq/g, SD 150 kBq/g) than in the manual approach (bias 17 kBq/g, SD 171 kBq/g). Possible reasons for these discrepancies include partial volume effects and discrepancies in the calibration of the methods.

Despite minor biases, the data-driven method offered superior scalability, robustness, and reproducibility, and was therefore used for all further image normalization in this study.

Method Box 3. Statistical Parametric Mapping (SPM) Applications

Objective: Detect significant voxel-wise correlations and group differences in PET images.

Application 1: Correlation Analysis (Image vs Vector)



Aim: Find voxels where PET signal intensity correlates significantly with *ex vivo* blood levels

Step 1: Preprocessing (registration of image to template, smoothing with Gaussian filter)

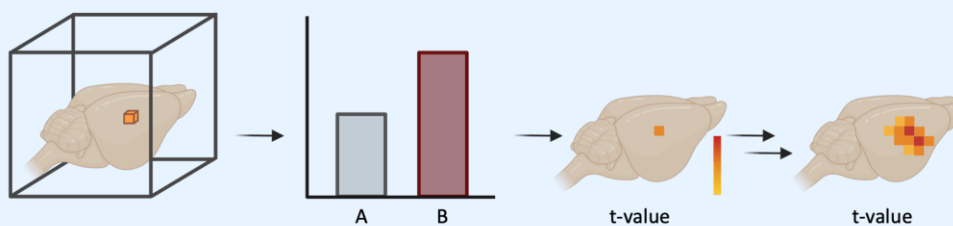
Step 2: Model design (PET signal as dependent, blood levels as predictor, statistical analysis: linear regression)

Step 3: Compute voxel-wise linear regression (t-values for each voxel)

Step 4: Generate statistical parametric map (each voxel is a significant t-value, higher t-value means a higher correlation)

Step 5: Apply multiple testing correction (e.g., False Discovery Rate or Bonferroni)

Application 2: Group comparison



Aim: Identify significant regional signal differences between groups

Step 1: Preprocessing as above

Step 2: Set up design matrix (group assignments)

Step 3: Perform voxel-wise group t-test or ANOVA

Step 4: Generate statistical parametric map (each voxel is a statistical value (e.g., t-value), higher t-value means a higher difference between groups)

Step 5: Apply multiple testing correction as above

Figure 13. Method Box 3. SPM applications used in this study. Created with BioRender.com.

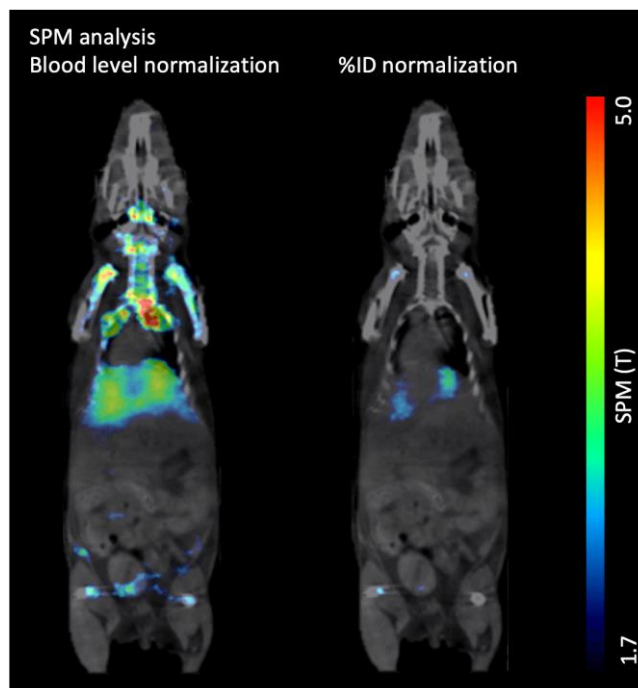


Figure 14. SPM maps were generated for group comparisons between WT and TREM2 KO mice ($n = 11$ each) of TREM2 PET images after normalization to blood levels and %ID, and overlaid onto a CT template. Two-sample t-test, $p < 0.05$. Adapted from (236), licensed under CC BY 4.0.

We next investigated whether blood-normalized or %ID-normalized PET images would lead to higher spatial differences in radioactivity signals in WT mice, which express a moderate amount of TREM2 on microglial cells in the brain and macrophages in the periphery, and TREM2 KO mice, which lack TREM2 expression (240). We used an SPM-based voxel-wise group comparison and found enhanced signal difference for blood level-normalized PET images, especially in the liver and bone, which are both organs that express TREM2 (53) (Figure 14).

Validation Using TREM2 Protein Expression

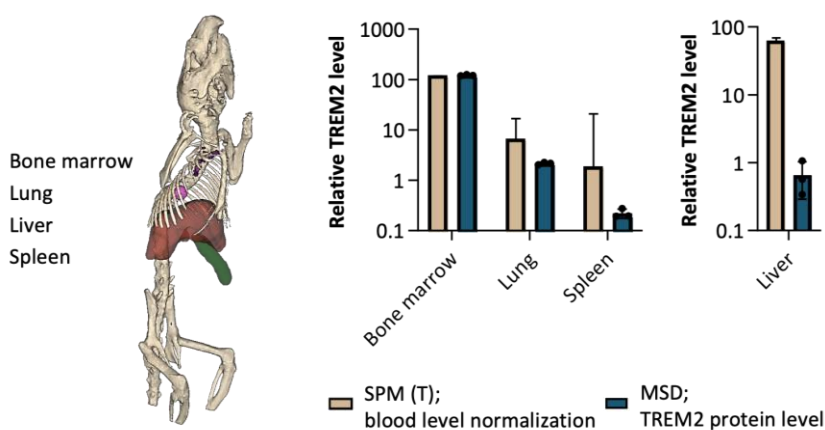


Figure 15. Schematic illustration of segmented organs. And a relative TREM2 comparison of SPM t-values of these organs, representing the difference of the group comparison between WT and TREM2 KO mice ($n = 11$ each) and

quantified TREM2 protein levels in WT mice ($n = 3$) by MSD analysis. Mean \pm SD. Adapted from (236), licensed under CC BY 4.0.

In order to validate the blood normalization method, we determined whether the observed enhanced PET signal differences in TREM2 radioligand between the two mouse groups reflected the actual biological TREM2 distribution. We compared the SPM-derived t-values from the group comparison (WT vs. TREM2 KO mice) of the bone marrow, lung, spleen and liver to TREM2 protein levels in WT mice measured by MSD (MesoScale Discovery, Maryland), an immunoassay that quantifies proteins.

Blood-normalized PET images exhibited higher t-values across all organs in comparison to %ID-normalized images (Figure 15). The t-values of the organs derived from blood-normalized PETs also demonstrated relative alignment with the TREM2 protein quantification for the bone marrow, lung and spleen and significantly correlated ($R^2 = 0.9990$, $p < 0.0001$, linear regression). The observed discrepancy in TREM2 radioligand intensity in these organs (a direct difference, no SPM analysis) among the PETs of the groups confirmed a significant correlation with TREM2 protein expression levels ($R^2 = 0.9950$, $p = 0.0451$, linear regression). However, it is important to acknowledge that the observed correlation was predominantly driven by bone marrow.

The t-value of the liver demonstrated a considerable elevation in relation to TREM2 protein quantification levels, which can be attributed to the predominance of excretion over specific TREM2 binding.

Application in an AD Mouse Model

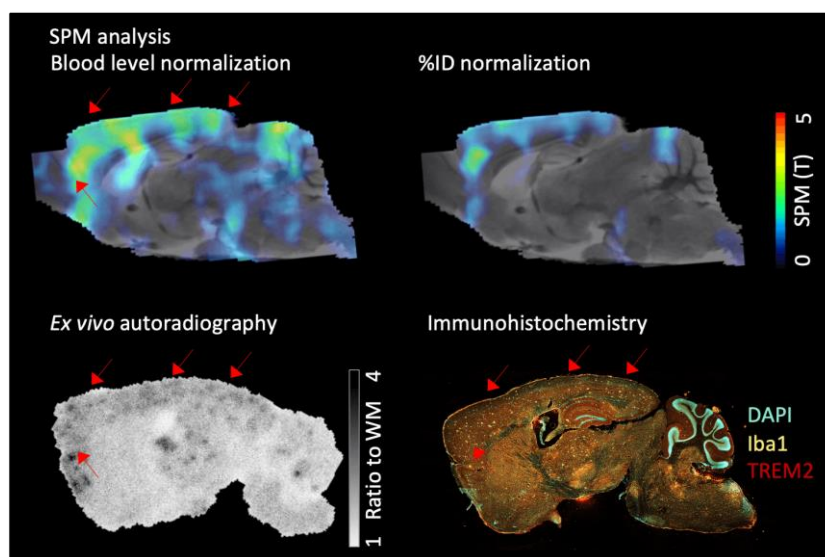


Figure 16. SPM maps were generated from group comparisons between WT;TfR^{mu/hu} and APP^{SAA};TfR^{mu/hu} mice ($n = 6$ each) of TREM2 PET images after normalization to blood levels and overlaid on an MRI template. Two-sample t-test, $p < 0.05$. Representative *ex vivo* autoradiography of a perfused APP^{SAA};TfR^{mu/hu} brain slice and immunohistochemistry of the adjacent brain slice (DNA (4',6-Diamidin-2-phenylindol, DAPI) in blue, microglia (ionized calcium-binding adapter molecule 1, Iba1) in yellow and TREM2 in red). Red arrows indicate increased TREM2 signals. Adapted from (236), licensed under CC BY 4.0.

Following the validation of blood normalization for TREM2 PET, we applied the method in a mouse model of amyloidosis ($APP^{SAA};TfR^{mu/hu}$) that expresses high TREM2 levels in comparison with WT; $TfR^{mu/hu}$ controls (181). We performed a second SPM group analysis to investigate the spatial differences between both groups using PET images that had been normalized to the blood level or %ID. Blood-normalized PET images exhibited stronger differences in the cortex and hippocampus, both high TREM2-expressing regions (234, 235), when compared to the %ID normalized images (Figure 16). *Ex vivo* autoradiography of $APP^{SAA};TfR^{mu/hu}$ confirmed a 2-fold signal difference between the cortex and basal-ganglia, and immunohistochemistry showed a 3-fold difference for TREM2 in the plaque-surrounding microglia. The localizations obtained from both methods aligned with the regions highlighted by SPM analysis after blood level normalization.

Application in a Myocardial Infarction Mouse Model

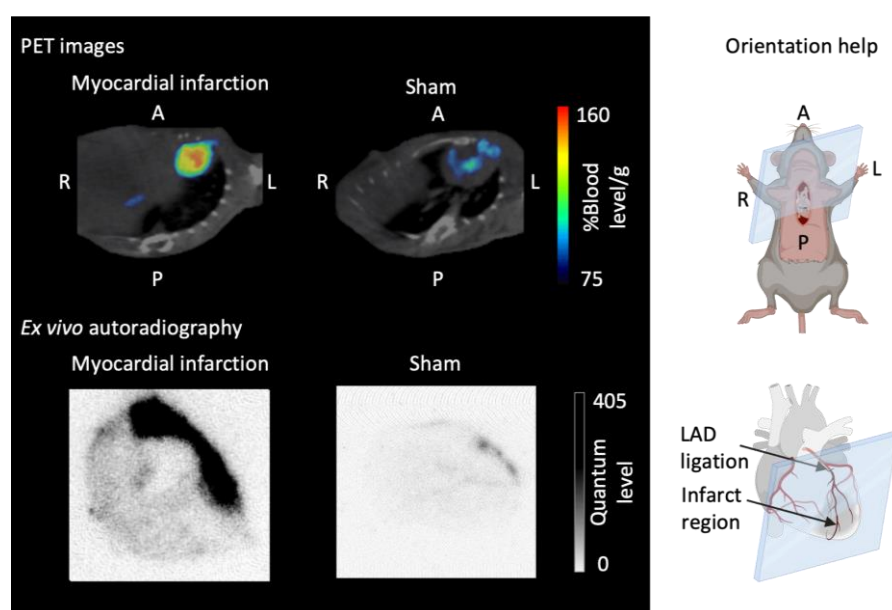


Figure 17. Representative PET images (overlaid onto a CT) and correlating autoradiography images of the infarct region in the heart of a left anterior descending artery-(LAD)-ligated WT mouse (myocardial infarction model) and the same region in the heart of a sham-operated WT mouse. Illustrations show the planes of the images and are shown for orientation. Created with BioRender.com. Adapted from (236), licensed under CC BY 4.0.

Our second disease model to apply the blood normalization method was a mouse model of myocardial infarction. TREM2 PET was performed in WT mice ($n = 6$) five days after left anterior descending artery (LAD) ligation, which causes oxygen deprivation (243). Four sham-operated mice were used as controls. *Ex vivo* autoradiography of the infarcted region of the heart was performed on day seven after surgery, as high TREM2 expression has been reported in literature in the infarcted region of LAD-ligated mice between days five and seven after surgery (244, 245). PET images and corresponding *ex vivo* autoradiography demonstrated strong TREM2 radioligand accumulation in the infarcted region and minimal signal in sham mice (Figure 17). The variability in TREM2 radioligand intensity in the infarcted region is probably due to ligation place-

ment, resulting in variable infarct sizes (246). The signal intensity in infarcted zones in PET correlated more strongly with *ex vivo* autoradiography when blood normalization was used, confirming the superiority of this method also in the second disease mouse model. Blood levels were segmented from the carotid artery in this case, to avoid potential spill-overs from the infarcted heart tissue.

Throughout the study, image-derived blood levels did not show significant differences between the compared mouse cohorts, suggesting that pathological changes in blood radioligand levels were minimal in our study.

The results were published in my second first-author paper, "*Image-Derived Blood Normalization of Antibody-Based TREM2 PET in Mouse Models of Amyloidosis and Myocardial Infarction*" (236), in *The Journal of Nuclear Medicine* in July 2025.

5. Conclusion and Outlook

AD poses a great threat to our society. While it takes approximately two hours to read this thesis, 1440 individuals worldwide developed AD during that time, highlighting the urgency for novel diagnostic and therapeutic strategies.

This thesis presents the first microglia-specific PET radioligand capable of visualizing TREM2-expressing microglia in mouse models of AD and TREM2-expressing macrophages in a myocardial infarction model. Integration of the brain-shuttle technology (in this case, ATV) into the radioligand design enabled efficient BBB penetration, allowing CNS access of an antibody-based radioligand, an important step toward broadening this technology in molecular imaging.

Additionally, we conducted *in vivo* autoradiography and immunohistochemistry studies targeting human TREM2. These early translational data are promising and support the transition to clinical PET applications.

Furthermore, we demonstrated that enhanced detection and quantification of TREM2 is possible when PET images are normalized to account for the blood levels.

A central aim was to develop a radioligand capable of detecting TREM2 *in vivo*. We achieved this by demonstrating that the bispecific radioligand [⁶⁴Cu]Cu-NODAGA-ATV:4D9 enabled the visualization of activated microglia in AD mouse models and, notably, TREM2-expressing peripheral macrophages in a myocardial infarction model. The ATV system proved to be essential, facilitating a 4.6-fold increase in brain uptake. Preliminary human tissue experiments further support the clinical relevance of TREM2 targeting radioligands.

The second major aim was to improve the quantitative PET analysis. We hypothesized that normalizing PET images to radioligand blood levels, rather than standard %ID normalization, would provide a more biologically accurate representation of the TREM2 expression. This hypothesis was fully supported by our data, both in terms of increased signals in pathologically TREM2-rich regions and correlation with protein levels in relevant organs.

Implications of this work: TREM2 PET opens new possibilities for the selective imaging of microglial activation. Currently available radioligands, such as those targeting TSPO, lack the necessary specificity to visualize these activation states selectively. Brain shuttle technology, which is already used for therapeutic antibody delivery, has now been proven successful in PET imaging as well, making antibody-based radioligands with target regions in the brain more attractive. Our results also emphasize the importance of image normalization to blood levels, especially for molecules with slow pharmacokinetics, such as antibodies. This insight enables the re-evaluation of existing imaging datasets with improved accuracy.

While the translational potential is clear, some limitations must be considered. The [⁶⁴Cu]Cu-NODAGA-ATV:4D9 radioligand binds to both TREM2 (including soluble TREM2) and hTfR, with the latter accounting for a substantial fraction of the total brain uptake. Adjusting the affinity

ratios or increasing the molar activity may help future studies to improve TREM2 PET. Additionally, differences between human and murine TREM2 expression must be considered, as well as the anatomical challenges of PET in small animal brains, where spill-overs from the skull may affect accuracy more than in humans.

The study also used whole blood radioligand levels for normalization, which may not fully reflect the unbound radioligand available in the plasma. Although no significant differences in blood levels were observed between the groups, it remains unclear whether this reflects true biological realities or opposing effects canceling each other out.

This research process also brought some unexpected findings. While the brain shuttle improved brain uptake, it did not proportionally increase the amount of TREM2-specific signals. Future designs could adjust the antibody affinities or explore alternative shuttle systems. Additionally, we encountered variability in infarct size in the myocardial model, highlighting the need for precise standardization of disease induction protocols.

Despite these challenges, our study lays a solid foundation for future TREM2 PET imaging. Longitudinal studies will be essential to assess whether this radioligand can effectively track microglial activation and therapeutic responses over time. Its potential use in clinical trials, particularly those involving anti-inflammatory or anti-A β therapies, appears promising.

We have recently started TREM2 PET in patients, with the radiochemical translation successfully conducted by the author. The first clinical results are expected soon and will shed light on the future potential of TREM2 PET.

6. Publications

6.1 List of Publications

Articles

The following research articles are summarized to a cumulative dissertation in this thesis:

1. Monireh Shojaei*, Rebecca Schaefer*, Kai Schlepckow, Lea H. Kunze, Felix L. Struebing, Bettina Brunner, Michael Willem, Laura M. Bartos, Astrid Feiten, Giovanna Palumbo, Thomas Arzberger, Peter Bartenstein, Gian C. Parico, Dan Xia, Kathryn M. Monroe, Christian Haass, Matthias Brendel*, Simon Lindner*: **PET imaging of microglia in Alzheimer's disease using copper-64 labeled TREM2 antibodies**
Theranostics, 2024, doi: 10.7150/thno.97149 (IF 13.3)
*contributed equally
2. Rebecca Schaefer, Lea H. Kunze, Marlies Haertel, Yeqian Zhu, Kai Schlepckow, Michael Willem, Laura M. Bartos, Giovanna Palumbo, Lukas Tomas, Christian Schulz, Steffen Massberg, Rudolf A. Werner, Maximilian Fischer, Dan Xia, Kathryn M. Monroe, Christian Haass, Matthias Brendel*, Simon Lindner*: **Image-Derived Blood Normalization of Antibody-Based TREM2 PET in Mouse Models of Amyloidosis and Myocardial Infarction**
Journal of Nuclear Medicine, 2025, doi: 10.2967/jnumed.125.269472 (IF 9.1)

Further articles, which are not part of the thesis:

Jonathan A. Gernert*, Laura Sanzo*, Hanna Zimmermann, Franziska Thaler, Letizia Vogler, Johannes S. Gnörich, Lisa Tagnin, Simon Lindner, Benjamin Kugelmann, Rebecca Schaefer, Gerard N. Bischof, Sabrina Katzdobler, Rudolf A. Werner, Günter U. Höglinger, Johannes Levin, Nicolai Franzmeier, Boris Rauchmann, Robert Perneczky, Martin Kerschensteiner, Tania Kümpfel*, Matthias Brendel*: **[¹⁸F]fluorodeprenyl-D2 PET for assessment and monitoring of astrogliosis in anti-LGI1-IgG Autoimmune Encephalitis**
Submitted to EJNMMI (f84957f9bcce112d) (IF 7.6)

Emanuel Joseph, Lea H. Kunze, Rebecca Schaefer, Giovanna Palumbo, Benjamin Kugelmann, Stephan Wagner, Sven Lammich, Regina Feederle, Michael Willem, Rudolf A. Werner, Matthias Brendel, Simon Lindner: **Design, Synthesis and Preclinical Evaluation of a brain-permeable PET Tracer for P2Y₁₂R Imaging in the Brain**
Journal of Medicinal Chemistry, 2025, doi: 10.1021/acs.jmedchem.5c00457 (IF 6.8)

Melissa J. Antons, Sandra Kloiber-Langhorst, Heidrun Hirner-Eppeneder, [Rebecca Schaefer](#), Jennifer Stueckl, Giovanna Palumbo, Rosel Oos, Felix Herr, Simon Lindner, Sibylle Ziegler, Matthias Brendel, Jens Ricke, Maurice M. Heimer*, Clemens C. Cyran*: **[¹⁸F]FDG-PET/CT imaging for response characterization of experimental melanomas to anti-PD-L1/anti-CTLA-4 immunotherapy**

Submitted to Molecular Imaging and Biology (63843b33d7a85e70) (IF 2.5)

Lea H. Kunze, Giovanna Palumbo, Johannes Gnörich, Karin Wind-Mark, [Rebecca Schaefer](#), Simon Lindner, Franz-Josef Gildehaus, Sibylle Ziegler, Matthias Brendel: **Fibrillar amyloidosis and synaptic vesicle protein expression progress jointly in the cortex of a mouse model with β -amyloid pathology**

NeuroImage, 2025, doi: 10.1016/j.neuroimage.2025.121165 (IF 4.5)

Laura M. Bartos, Sebastian T. Kunte, Stephan Wagner, Philipp Beumers, [Rebecca Schaefer](#), Artem Zatcepin, Yunlei Li, Maria Griessl, Leonie Hoermann, Karin Wind-Mark, Peter Bartenstein, Sabina Tahirovic, Sibylle Ziegler, Matthias Brendel, Johannes Gnörich: **Astroglial glucose uptake determines brain FDG-PET alterations and metabolic connectivity during healthy aging in mice**

NeuroImage, 2024, doi: 10.1016/j.neuroimage.2024.120860 (IF 4.5)

Monireh Shojaei, Qihui Zhou, Giovanna Palumbo, [Rebecca Schaefer](#), Janne Kaskinoro, Pirjo Vehmaan-Kreula, Peter Bartenstein, Matthias Brendel, Dieter Edbauer, Simon Lindner: **Development and Preclinical Evaluation of a Copper-64-Labeled Antibody Targeting Glycine-Alanine Dipeptides for PET Imaging of C9orf72-Associated Amyotrophic Lateral Sclerosis/Frontotemporal Dementia**

ACS Pharmacology & Translational Science Journal, 2024, doi: 10.1021/acspsci.4c00037 (IF 3.7)

Maria Meindl, Artem Zatcepin, Johannes Gnörich, Maximilian Scheifele, Mirlind Zaganjori, Mattes Groß, Simon Lindner, [Rebecca Schaefer](#), Marcel Simmet, Sebastian Roemer, Sabrina Katzdobler, Johannes Levin, Günter Höglinger, Ann-Cathrin Bischof, Henryk Barthel, Osama Sabri, Peter Bartenstein, Thomas Saller, Nicolai Franzmeier, Sibylle Ziegler, Matthias Brendel: **Assessment of [¹⁸F]PI-2620 Tau-PET Quantification via Non-Invasive Automated Image Derived Input Function**

European Journal of Nuclear Medicine and Molecular Imaging, 2024, doi: 10.1007/s00259-024-06741-7 (IF 7.6)

Laura M. Bartos, Sabrina V. Kirchleitner, Zeynep Ilgin Kolabas, Stefanie Quach, Alexander Beck, Julia Lorenz, Jens Blobner, Stephan A. Mueller, Selin Ulukaya, Luciano Hoehner, Izabela Horvath, Karin Wind-Mark, Adrien Holzgreve, Viktoria C. Ruf, Lukas Gold, Lea H. Kunze, Sebastian T.

Kunte, Philipp Beumers, Ha Eun Park, Melissa Antons, Artem Zatcepin, Nils Briel, Leonie Hoermann, [Rebecca Schaefer](#), Denise Messerer, Peter Bartenstein, Markus J. Riemenschneider, Simon Lindner, Sibylle Ziegler, Jochen Herms, Stefan F. Lichtenthaler, Ali Ertürk, Joerg C. Tonn, Louisa von Baumgarten, Nathalie L. Albert*, Matthias Brendel*: **Deciphering sources of PET signals in the tumor microenvironment of glioblastoma at cellular resolution**

Science Advances, 2023, doi: 10.1126/sciadv.adi8986 (IF 11.7)

*contributed equally

Oral Presentations

[Rebecca Schaefer](#), Lea H. Kunze, Kai Schlepckow, Michael Willem, Marlies Hartel, Laura M. Bartos, Franz J. Gildehaus, Giovanna Palumbo, Dan Xia, Kathryn M. Monroe, Christian Haass, Matthias Brendel, Simon Lindner: **Evaluation of Antibody-based TREM2 PET in mice: Contrasting Image-Derived Blood Normalization with the Standard %ID Normalization Method**

26th International Symposium on Radiopharmaceutical Sciences, Gold Coast, Queensland May 11-15, 2025

Marlies Haertel, [Rebecca Schaefer](#), Ha Eun Park, Leonie Hoermann, Kai Schlepckow, Christian Haass, Joseph W. Lewcock, Kathryn M. Monroe, Nathalie L. Albert, Louisa von Baumgarten, Sibylle Ziegler, Simon Lindner, Matthias Brendel, Laura M. Bartos: **PET imaging using a Copper-64 labeled TREM2 antibody with blood-brain barrier transport vehicle facilitates selective assessment of tumor associated immune cells in glioblastoma mice**

EANM Congress 2024, Hamburg, Germany, October 19-23, 2024

[Rebecca Schaefer](#), Marlies Haertel, Lea H. Kunze, Laura M. Bartos, Giovanna Palumbo, Kai Schlepckow, Christian Haass, Joseph W. Lewcock, Kathryn M. Monroe, Matthias Brendel, Simon Lindner: **Evaluating the cellular binding specificity of a copper-64 labelled antibody transport vehicle enabled TREM2 PET tracer using scRadiotracing in mice**

Annual Meeting of the German Pharmaceutical Society, DPhG, Münster, Germany, September 23-26, 2024

[Rebecca Schaefer](#), Giovanna Palumbo, Kai Schlepckow, Kathryn M. Monroe, Christian Haass, Peter Bartenstein, Matthias Brendel, Simon Lindner: **scRadiotracing: Eine neue Methode zum Nachweis zellspezifischen Tracer-Uptakes**

29th Annual Meeting of the AGRR, Bad Salzflun, Germany, September 28-30, 2023

Laura Sanzo, Jonathan Gernert, Letizia Vogler, Mirlind Zaganjori, Simon Lindner, Rebecca Schäfer, Andrew Stephens, Martin Kerschensteiner, Tania Kümpfel, Matthias Brendel: **Assessment of [¹⁸F]D2-Deprenyl as an inflammation tracer in LGI1 positive limbic encephalitis**
SNMMI Annual Meeting, Chicago, Illinois, USA, June 24-27, 2023

Poster Presentation

Marlies Haertel, Rebecca Schaefer, Lea H. Kunze, Ha E. Park, Leonie Hoermann, Kai Schlepckow, Franz J. Gildehaus, Christian Haass, Joseph W. Lewcock, Kathryn M. Monroe, Nathalie L. Albert, Louisa von Baumgarten, Sibylle Ziegler, Simon Lindner, Matthias Brendel: **Blood-Brain Barrier Penetrating Copper-64 TREM2 Antibody Enables Targeted PET Imaging of Tumor-Associated Immune Cells in Glioblastoma Mouse Models**

26th International Symposium on Radiopharmaceutical Sciences, Gold Coast, Queensland May 11-15, 2025

Emanuel Joseph, Lea H. Kunze, Giovanna Palumbo, Rebecca Schäfer, Benjamin Kugelmann, Stephan Wagner, Sven Lammich, Regina Feederle, Michael Willem, Rudolph A. Werner, Franz Josef Gildehaus, Matthias Brendel, Simon Lindner: **Design, synthesis and preclinical evaluation of a novel brain-permeable P2Y₁₂R PET ligand**

26th International Symposium on Radiopharmaceutical Sciences, Gold Coast, Queensland May 11-15, 2025

Lisa Tagnin, Julia Dornreich, Marianthi Zeinaki, Letizia Vogler, Laura Sanzo, Sabrina Katzdobler, Alexander Jäck, Alexander Bernhardt, Boris Rauchmann, Sophia Stöcklein, Marcel Simmet, Emanuel Joseph, Simon Lindner, Rebecca Schäfer, Norman Koglin, Andre Mueller, Andrew W. Stephens, Jonathan Gernert, Franziska Hopfner, Günter Höglinger, Robert Pernecky, Tania Kümpfel, Martin Kerschensteiner, Franziska Thaler, Johannes Levin, Matthias Brendel: **Feasibility of Short Imaging Protocols for [¹⁸F]fluorodeprenyl-D2 PET in Autoimmune Encephalitis and Multiple System Atrophy**

63rd Annual Meeting of the DGN, Bremen, Germany April 2-5, 2025

Melissa Antons, Sandra Kloiber-Langhorst, Heidrun Hirner-Eppeneder, Rebecca Schaefer, Jennifer Stueckl, Giovanna Palumbo, Rosel Oos, Simon Lindner, Sibylle Ziegler, Matthias Brendel, Jens Ricke, Maurice Heimer, Clemens C. Cyran: **Multi-time-point [¹⁸F]FDG-PET/CT for monitoring a combined anti-PD-L1/anti-CTLA-4 immunotherapy in a murine melanoma model with multiparametric immunohistochemical validation**

EANM Congress 2024, Hamburg, Germany, October 19-23, 2024

6.2 Contribution to Paper I

“PET imaging of microglia in Alzheimer's disease using copper-64 labeled TREM2 antibodies.” (130)

The contribution to the first paper published in Theranostics is shown in the following table for better overview.

Table 2. Contributions to paper I.

Figure or Table	Contribution	Comment
Figure 2B	Data curation, Formal analysis	Re-analysis of data previously analyzed by Monireh Shojaei.
Figure 3B	Data curation, Formal analysis	-
Figure 6A-F	Conceptualization, Data curation, Formal analysis, Investigation, Methodology, Validation	Conceptualization together with Kathryn M. Monroe, Matthias Brendel and Simon Lindner. Investigation: Radioligand application together with Giovanna Palumbo.
Figure 7	Data curation, Formal analysis, Investigation, Methodology, Validation	Investigation and Methodology for Immunohistochemistry by Felix Struebing.
Figure S1	Data curation, Formal analysis, Investigation, Methodology, Validation	-
Figure S2 F+G	Conceptualization, Data curation, Formal analysis, Investigation, Methodology, Validation	Conceptualization together with Kathryn M. Monroe, Matthias Brendel and Simon Lindner.
Figure S3 B-D	Conceptualization, Data curation, Formal analysis, Investigation, Methodology, Validation	Conceptualization together with Kathryn M. Monroe, Matthias Brendel and Simon Lindner. Investigation: Radioligand application together with Giovanna Palumbo.

Figure S4	Conceptualization, Data curation, Formal analysis, Investigation, Methodology, Validation	Conceptualization together with Kathryn M. Monroe, Matthias Brendel and Simon Lindner. Investigation: Radioligand application together with Giovanna Palumbo.
Figure S5	Data curation, Formal analysis	Re-analysis of data previously analyzed by Monireh Shojaei.
Figure S6	Data curation, Formal analysis	-
Figure S8	Conceptualization, Data curation, Formal analysis, Investigation,	Conceptualization together with Kathryn M. Monroe, Matthias Brendel and Simon Lindner.
Figure S9	Conceptualization, Data curation, Formal analysis, Investigation, Methodology, Validation	Conceptualization together with Kathryn M. Monroe, Matthias Brendel and Simon Lindner. Investigation: Radioligand application together with Giovanna Palumbo.
Figure S10	Conceptualization, Data curation, Formal analysis, Investigation, Methodology, Validation	Conceptualization together with Kathryn M. Monroe, Matthias Brendel and Simon Lindner. Investigation: Radioligand application together with Giovanna Palumbo.
Table S1	Data curation, Formal analysis	Re-analysis of data previously analyzed by Monireh Shojaei.
Table S6	Conceptualization, Data curation, Formal analysis, Investigation,	Conceptualization together with Kathryn M. Monroe, Matthias Brendel and Simon Lindner.
Table S7	Conceptualization, Data curation, Formal analysis, Investigation,	Conceptualization together with Kathryn M. Monroe, Matthias Brendel and Simon Lindner.

Graphical Abstract	Visualization	-
Whole paper	Data interpretation, Visualization, Writing – review & editing	Data interpretation, Writing – review & editing together with Kai Schlepckow, Kathryn M. Monroe, Christian Haass, Matthias Brendel and Simon Lindner.

6.2.1 Rationale for shared first authorship

The results of two different PhD projects, each focusing on a different aspect of a shared topic area, were combined into a single publication with the aim of presenting a comprehensive narrative. The data collection for these projects was conducted independently by the respective PhD students. Monireh Shojaei's contributions included the development of the radioligand and the preliminary studies on radioligand distribution. My PhD project was built upon these foundations, with a focus on demonstrating the specificity of the radioligand for microglial cells. In addition, I played an instrumental role in the data analysis and interpretation, the review and editing process of the manuscript, ultimately leading the resubmission process.

6.3 Contribution to the Paper II

“Image-Derived Blood Normalization of Antibody-Based TREM2 PET in Mouse Models of Amyloidosis and Myocardial Infarction.” (236)

The contribution of the second paper published in the Journal of Nuclear Medicine was the idea of the study, leadership of investigation, methodology, formal analysis, data interpretation, data curation, project administration, and revision of the study on the normalization of TREM2 PET data. Initially, I synthesized the radioligand and conducted the mouse experiments (with technical assistance from Lea H. Kunze, Marlies Haertel, Laura Bartos, and Giovanna Palumbo; heart operations were performed by Yeqian Zhu, Dan Xia conducted the TREM2 protein quantification). I measured the radioactivity of the blood samples obtained using a gamma counter and analyzed them. I reconstructed and processed the acquired small-animal PET/CT data (including cropping, co-localization, transformation and normalization). The methodology for the protocol for PET/CT data analysis was developed in collaboration with Matthias Brendel. Next, I correlated the resulting PET data with the collected blood data or analyzed them in multiple linear regressions and group comparisons using SPM. Additionally, I segmented organ-specific radioactivity values from the mouse using Imalytics Preclinical Software. In this context, I was entrusted with the selection of suitable software and purchase of a license for the clinic. The creation

of all figures within the manuscript was my responsibility. The initial manuscript draft was authored by me and was subsequently corrected and expanded by my co-authors. Furthermore, I completed two rounds of revision.

7. Bibliography

1. Alzheimer's Disease International. World Alzheimer Report 2019: Attitudes to dementia. London: Alzheimer's Disease International; 2019 [cited 2025 Jun 29]. Available from: <https://www.alzint.org/u/WorldAlzheimerReport2019.pdf>.
2. Kumar A, Sidhu J, Lui F, Tsao JW. Alzheimer Disease. StatPearls. Treasure Island (FL): StatPearls Publishing Copyright © 2025, StatPearls Publishing LLC.; 2025.
3. Mielke MM. Sex and Gender Differences in Alzheimer's Disease Dementia. *Psychiatr Times*. 2018;35(11):14-7.
4. World Health Organization. Global status report on the public health response to dementia. Geneva: World Health Organization; 2021 [cited 2025 Jun 29]. Available from: <https://iris.who.int/bitstream/handle/10665/344701/9789240033245-eng.pdf>.
5. Nichols E, Steinmetz JD, Vollset SE, Fukutaki K, Chalek J, Abd-Allah F, et al. Estimation of the global prevalence of dementia in 2019 and forecasted prevalence in 2050: an analysis for the Global Burden of Disease Study 2019. *Lancet Public Health*. 2022;7(2):e105-e25.
6. Gustavsson A, Norton N, Fast T, Frölich L, Georges J, Holzapfel D, et al. Global estimates on the number of persons across the Alzheimer's disease continuum. *Alzheimers Dement*. 2023;19(2):658-70.
7. Wong W. Economic burden of Alzheimer disease and managed care considerations. *Am J Manag Care*. 2020;26(8 Suppl):S177-s83.
8. Alzheimer's Association. What is Alzheimer's disease? Alzheimer's Association; (c2025) [cited 2025 Jun 29]. Available from: <https://www.alz.org/alzheimers-dementia/what-is-alzheimers>.
9. Kawaharada R, Sugimoto T, Matsuda N, Tsuboi Y, Sakurai T, Ono R. Impact of loss of independence in basic activities of daily living on caregiver burden in patients with Alzheimer's disease: A retrospective cohort study. *Geriatr Gerontol Int*. 2019;19(12):1243-7.
10. Desai AK, Grossberg GT, Sheth DN. Activities of daily living in patients with dementia: clinical relevance, methods of assessment and effects of treatment. *CNS Drugs*. 2004;18(13):853-75.
11. Sims JR, Zimmer JA, Evans CD, Lu M, Ardayfio P, Sparks J, et al. Donanemab in Early Symptomatic Alzheimer Disease: The TRAILBLAZER-ALZ 2 Randomized Clinical Trial. *Jama*. 2023;330(6):512-27.
12. van Dyck CH, Swanson CJ, Aisen P, Bateman RJ, Chen C, Gee M, et al. Lecanemab in Early Alzheimer's Disease. *N Engl J Med*. 2023;388(1):9-21.
13. Birks JS, Harvey RJ. Donepezil for dementia due to Alzheimer's disease. *Cochrane Database Syst Rev*. 2018;6(6):Cd001190.
14. Birks JS, Grimley Evans J. Rivastigmine for Alzheimer's disease. *Cochrane Database Syst Rev*. 2015(4):Cd001191.
15. Raskind MA, Peskind ER, Wessel T, Yuan W. Galantamine in AD: A 6-month randomized, placebo-controlled trial with a 6-month extension. The Galantamine USA-1 Study Group. *Neurology*. 2000;54(12):2261-8.
16. Reisberg B, Doody R, Stöffler A, Schmitt F, Ferris S, Möbius HJ. Memantine in moderate-to-severe Alzheimer's disease. *N Engl J Med*. 2003;348(14):1333-41.
17. Jack CR, Jr., Andrews JS, Beach TG, Buracchio T, Dunn B, Graf A, et al. Revised criteria for diagnosis and staging of Alzheimer's disease: Alzheimer's Association Workgroup. *Alzheimers Dement*. 2024;20(8):5143-69.
18. Dubois B, Villain N, Frisoni GB, Rabinovici GD, Sabbagh M, Cappa S, et al. Clinical diagnosis of Alzheimer's disease: recommendations of the International Working Group. *Lancet Neurol*. 2021;20(6):484-96.

19. Heneka MT, Carson MJ, El Khoury J, Landreth GE, Brosseron F, Feinstein DL, et al. Neuroinflammation in Alzheimer's disease. *Lancet Neurol.* 2015;14(4):388-405.
20. Calsolaro V, Edison P. Neuroinflammation in Alzheimer's disease: Current evidence and future directions. *Alzheimers Dement.* 2016;12(6):719-32.
21. Lewcock JW, Schlepckow K, Di Paolo G, Tahirovic S, Monroe KM, Haass C. Emerging Microglia Biology Defines Novel Therapeutic Approaches for Alzheimer's Disease. *Neuron.* 2020;108(5):801-21.
22. Si ZZ, Zou CJ, Mei X, Li XF, Luo H, Shen Y, et al. Targeting neuroinflammation in Alzheimer's disease: from mechanisms to clinical applications. *Neural Regen Res.* 2023;18(4):708-15.
23. Alzheimer A, Stelzmann RA, Schnitzlein HN, Murtagh FR. An English translation of Alzheimer's 1907 paper, "Über eine eigenartige Erkrankung der Hirnrinde". *Clin Anat.* 1995;8(6):429-31.
24. Overk CR, Masliah E. Pathogenesis of synaptic degeneration in Alzheimer's disease and Lewy body disease. *Biochem Pharmacol.* 2014;88(4):508-16.
25. Forner S, Baglietto-Vargas D, Martini AC, Trujillo-Estrada L, LaFerla FM. Synaptic Impairment in Alzheimer's Disease: A Dysregulated Symphony. *Trends Neurosci.* 2017;40(6):347-57.
26. Perl DP. Neuropathology of Alzheimer's disease. *Mt Sinai J Med.* 2010;77(1):32-42.
27. Dickson DW. Neuropathological diagnosis of Alzheimer's disease: a perspective from longitudinal clinicopathological studies. *Neurobiol Aging.* 1997;18(4 Suppl):S21-6.
28. DeTure MA, Dickson DW. The neuropathological diagnosis of Alzheimer's disease. *Mol Neurodegener.* 2019;14(1):32.
29. Karran E, Mercken M, De Strooper B. The amyloid cascade hypothesis for Alzheimer's disease: an appraisal for the development of therapeutics. *Nat Rev Drug Discov.* 2011;10(9):698-712.
30. Hardy JA, Higgins GA. Alzheimer's disease: the amyloid cascade hypothesis. *Science.* 1992;256(5054):184-5.
31. Barage SH, Sonawane KD. Amyloid cascade hypothesis: Pathogenesis and therapeutic strategies in Alzheimer's disease. *Neuropeptides.* 2015;52:1-18.
32. Leng F, Edison P. Neuroinflammation and microglial activation in Alzheimer disease: where do we go from here? *Nat Rev Neurol.* 2021;17(3):157-72.
33. Cai Y, Liu J, Wang B, Sun M, Yang H. Microglia in the Neuroinflammatory Pathogenesis of Alzheimer's Disease and Related Therapeutic Targets. *Front Immunol.* 2022;13:856376.
34. Miao J, Ma H, Yang Y, Liao Y, Lin C, Zheng J, et al. Microglia in Alzheimer's disease: pathogenesis, mechanisms, and therapeutic potentials. *Front Aging Neurosci.* 2023;15:1201982.
35. Chen Y, Yu Y. Tau and neuroinflammation in Alzheimer's disease: interplay mechanisms and clinical translation. *J Neuroinflammation.* 2023;20(1):165.
36. Hampel H, Hardy J, Blennow K, Chen C, Perry G, Kim SH, et al. The Amyloid- β Pathway in Alzheimer's Disease. *Mol Psychiatry.* 2021;26(10):5481-503.
37. Palmqvist S, Schöll M, Strandberg O, Mattsson N, Stomrud E, Zetterberg H, et al. Earliest accumulation of β -amyloid occurs within the default-mode network and concurrently affects brain connectivity. *Nat Commun.* 2017;8(1):1214.
38. Preston AR, Eichenbaum H. Interplay of hippocampus and prefrontal cortex in memory. *Curr Biol.* 2013;23(17):R764-73.
39. Euston DR, Gruber AJ, McNaughton BL. The role of medial prefrontal cortex in memory and decision making. *Neuron.* 2012;76(6):1057-70.
40. Braak H, Braak E. Frequency of stages of Alzheimer-related lesions in different age categories. *Neurobiol Aging.* 1997;18(4):351-7.
41. Thal DR, Rüb U, Orantes M, Braak H. Phases of A beta-deposition in the human brain and its relevance for the development of AD. *Neurology.* 2002;58(12):1791-800.

42. Colonna M, Butovsky O. Microglia Function in the Central Nervous System During Health and Neurodegeneration. *Annu Rev Immunol.* 2017;35:441-68.
43. Salter MW, Stevens B. Microglia emerge as central players in brain disease. *Nat Med.* 2017;23(9):1018-27.
44. Augusto-Oliveira M, Arrifano GP, Lopes-Araújo A, Santos-Sacramento L, Takeda PY, Anthony DC, et al. What Do Microglia Really Do in Healthy Adult Brain? *Cells.* 2019;8(10).
45. Gao C, Jiang J, Tan Y, Chen S. Microglia in neurodegenerative diseases: mechanism and potential therapeutic targets. *Signal Transduct Target Ther.* 2023;8(1):359.
46. Borst K, Dumas AA, Prinz M. Microglia: Immune and non-immune functions. *Immunity.* 2021;54(10):2194-208.
47. Deczkowska A, Keren-Shaul H, Weiner A, Colonna M, Schwartz M, Amit I. Disease-Associated Microglia: A Universal Immune Sensor of Neurodegeneration. *Cell.* 2018;173(5):1073-81.
48. Keren-Shaul H, Spinrad A, Weiner A, Matcovitch-Natan O, Dvir-Szternfeld R, Ulland TK, et al. A Unique Microglia Type Associated with Restricting Development of Alzheimer's Disease. *Cell.* 2017;169(7):1276-90.e17.
49. Cherry JD, Olschowka JA, O'Banion MK. Neuroinflammation and M2 microglia: the good, the bad, and the inflamed. *J Neuroinflammation.* 2014;11:98.
50. Paolicelli RC, Sierra A, Stevens B, Tremblay ME, Aguzzi A, Ajami B, et al. Microglia states and nomenclature: A field at its crossroads. *Neuron.* 2022;110(21):3458-83.
51. Hansen DV, Hanson JE, Sheng M. Microglia in Alzheimer's disease. *J Cell Biol.* 2018;217(2):459-72.
52. Ebrahimi R, Shahrokhi Nejad S, Falah Tafti M, Karimi Z, Sadr SR, Ramadhan Hussein D, et al. Microglial activation as a hallmark of neuroinflammation in Alzheimer's disease. *Metab Brain Dis.* 2025;40(5):207.
53. Colonna M. The biology of TREM receptors. *Nat Rev Immunol.* 2023;23(9):580-94.
54. Wang X, Wang Y, Yang L, Zhang Y, Yang L. TREM2⁺ macrophages: a key role in disease development. *Front Immunol.* 2025;16:1550893.
55. Bharadwaj S, Groza Y, Mierzwicka JM, Malý P. Current understanding on TREM-2 molecular biology and physiopathological functions. *Int Immunopharmacol.* 2024;134:112042.
56. Ulland TK, Colonna M. TREM2 - a key player in microglial biology and Alzheimer disease. *Nat Rev Neurol.* 2018;14(11):667-75.
57. Jay TR, von Saucken VE, Landreth GE. TREM2 in Neurodegenerative Diseases. *Mol Neurodegener.* 2017;12(1):56.
58. Ulland TK, Song WM, Huang SC, Ulrich JD, Sergushichev A, Beatty WL, et al. TREM2 Maintains Microglial Metabolic Fitness in Alzheimer's Disease. *Cell.* 2017;170(4):649-63.e13.
59. Konishi H, Kiyama H. Microglial TREM2/DAP12 Signaling: A Double-Edged Sword in Neural Diseases. *Front Cell Neurosci.* 2018;12:206.
60. Deczkowska A, Weiner A, Amit I. The Physiology, Pathology, and Potential Therapeutic Applications of the TREM2 Signaling Pathway. *Cell.* 2020;181(6):1207-17.
61. Zhao N, Bu G. A TREM2 antibody energizes microglia. *Nat Neurosci.* 2023;26(3):366-8.
62. Thornton P, Sevalle J, Deery MJ, Fraser G, Zhou Y, Ståhl S, et al. TREM2 shedding by cleavage at the H157-S158 bond is accelerated for the Alzheimer's disease-associated H157Y variant. *EMBO Mol Med.* 2017;9(10):1366-78.
63. Feuerbach D, Schindler P, Barske C, Joller S, Beng-Louka E, Worringer KA, et al. ADAM17 is the main sheddase for the generation of human triggering receptor expressed in myeloid cells (hTREM2) ectodomain and cleaves TREM2 after Histidine 157. *Neurosci Lett.* 2017;660:109-14.
64. Schlepckow K, Kleinberger G, Fukumori A, Feederle R, Lichtenthaler SF, Steiner H, et al. An Alzheimer-associated TREM2 variant occurs at the ADAM cleavage site and affects shedding and phagocytic function. *EMBO Mol Med.* 2017;9(10):1356-65.

65. Wang L, Nykänen NP, Western D, Gorijala P, Timsina J, Li F, et al. Proteo-genomics of soluble TREM2 in cerebrospinal fluid provides novel insights and identifies novel modulators for Alzheimer's disease. *Mol Neurodegener.* 2024;19(1):1.
66. Dhandapani R, Neri M, Bernhard M, Brzak I, Schweizer T, Rudin S, et al. Sustained Trem2 stabilization accelerates microglia heterogeneity and A β pathology in a mouse model of Alzheimer's disease. *Cell Rep.* 2022;39(9):110883.
67. Zhong L, Xu Y, Zhuo R, Wang T, Wang K, Huang R, et al. Soluble TREM2 ameliorates pathological phenotypes by modulating microglial functions in an Alzheimer's disease model. *Nature Commun.* 2019;10(1):1365.
68. Zhong L, Chen XF, Wang T, Wang Z, Liao C, Wang Z, et al. Soluble TREM2 induces inflammatory responses and enhances microglial survival. *J Exp Med.* 2017;214(3):597-607.
69. Wu K, Byers DE, Jin X, Agapov E, Alexander-Brett J, Patel AC, et al. TREM-2 promotes macrophage survival and lung disease after respiratory viral infection. *J Exp Med.* 2015;212(5):681-97.
70. Pascoal TA, Benedet AL, Ashton NJ, Kang MS, Therriault J, Chamoun M, et al. Microglial activation and tau propagate jointly across Braak stages. *Nat Med.* 2021;27(9):1592-9.
71. Deming Y, Filipello F, Cignarella F, Cantoni C, Hsu S, Mikesell R, et al. The MS4A gene cluster is a key modulator of soluble TREM2 and Alzheimer's disease risk. *Sci Transl Med.* 2019;11(505).
72. Suárez-Calvet M, Kleinberger G, Araque Caballero M, Brendel M, Rominger A, Alcolea D, et al. sTREM2 cerebrospinal fluid levels are a potential biomarker for microglia activity in early-stage Alzheimer's disease and associate with neuronal injury markers. *EMBO Mol Med.* 2016;8(5):466-76.
73. Piccio L, Deming Y, Del-Águila JL, Ghezzi L, Holtzman DM, Fagan AM, et al. Cerebrospinal fluid soluble TREM2 is higher in Alzheimer disease and associated with mutation status. *Acta Neuropathol.* 2016;131(6):925-33.
74. Heslegrave A, Heywood W, Paterson R, Magdalinou N, Svensson J, Johansson P, et al. Increased cerebrospinal fluid soluble TREM2 concentration in Alzheimer's disease. *Mol Neurodegener.* 2016;11:3.
75. Hickman SE, Kingery ND, Ohsumi TK, Borowsky ML, Wang LC, Means TK, et al. The microglial sensome revealed by direct RNA sequencing. *Nat Neurosci.* 2013;16(12):1896-905.
76. Hickman SE, El Khoury J. TREM2 and the neuroimmunology of Alzheimer's disease. *Biochem Pharmacol.* 2014;88(4):495-8.
77. Forabosco P, Ramasamy A, Trabzuni D, Walker R, Smith C, Bras J, et al. Insights into TREM2 biology by network analysis of human brain gene expression data. *Neurobiol Aging.* 2013;34(12):2699-714.
78. Hu N, Tan MS, Yu JT, Sun L, Tan L, Wang YL, et al. Increased expression of TREM2 in peripheral blood of Alzheimer's disease patients. *J Alzheimers Dis.* 2014;38(3):497-501.
79. Tserel L, Kolde R, Rebane A, Kisand K, Org T, Peterson H, et al. Genome-wide promoter analysis of histone modifications in human monocyte-derived antigen presenting cells. *BMC Genomics.* 2010;11:642.
80. Takahashi K, Rochford CD, Neumann H. Clearance of apoptotic neurons without inflammation by microglial triggering receptor expressed on myeloid cells-2. *J Exp Med.* 2005;201(4):647-57.
81. Gonçalves LA, Rodrigues-Duarte L, Rodo J, Vieira de Moraes L, Marques I, Penha-Gonçalves C. TREM2 governs Kupffer cell activation and explains belr1 genetic resistance to malaria liver stage infection. *Proc Natl Acad Sci U S A.* 2013;110(48):19531-6.
82. Paloneva J, Mandelin J, Kiialainen A, Bohling T, Prudlo J, Hakola P, et al. DAP12/TREM2 deficiency results in impaired osteoclast differentiation and osteoporotic features. *J Exp Med.* 2003;198(4):669-75.
83. Guerreiro R, Wojtas A, Bras J, Carrasquillo M, Rogaeva E, Majounie E, et al. TREM2 variants in Alzheimer's disease. *N Engl J Med.* 2013;368(2):117-27.
84. Jonsson T, Stefansson H, Steinberg S, Jonsdottir I, Jonsson PV, Snaedal J, et al. Variant of TREM2 associated with the risk of Alzheimer's disease. *N Engl J Med.* 2013;368(2):107-16.
85. Wang Y, Cella M, Mallinson K, Ulrich JD, Young KL, Robinette ML, et al. TREM2 lipid sensing sustains the microglial response in an Alzheimer's disease model. *Cell.* 2015;160(6):1061-71.

86. Song W, Hooli B, Mullin K, Jin SC, Cella M, Ulland TK, et al. Alzheimer's disease-associated TREM2 variants exhibit either decreased or increased ligand-dependent activation. *Alzheimers Dement*. 2017;13(4):381-7.
87. Atagi Y, Liu CC, Painter MM, Chen XF, Verbeeck C, Zheng H, et al. Apolipoprotein E Is a Ligand for Triggering Receptor Expressed on Myeloid Cells 2 (TREM2). *J Biol Chem*. 2015;290(43):26043-50.
88. Bailey CC, DeVaux LB, Farzan M. The Triggering Receptor Expressed on Myeloid Cells 2 Binds Apolipoprotein E. *J Biol Chem*. 2015;290(43):26033-42.
89. Zhou Y, Song WM, Andhey PS, Swain A, Levy T, Miller KR, et al. Human and mouse single-nucleus transcriptomics reveal TREM2-dependent and TREM2-independent cellular responses in Alzheimer's disease. *Nat Med*. 2020;26(1):131-42.
90. Guerreiro R, Hardy J. Genetics of Alzheimer's disease. *Neurotherapeutics*. 2014;11(4):732-7.
91. Lee CYD, Daggett A, Gu X, Jiang LL, Langfelder P, Li X, et al. Elevated TREM2 Gene Dosage Reprograms Microglia Responsivity and Ameliorates Pathological Phenotypes in Alzheimer's Disease Models. *Neuron*. 2018;97(5):1032-48.e5.
92. Vicente-Rodríguez M, Singh N, Turkheimer F, Peris-Yague A, Randall K, Veronese M, et al. Resolving the cellular specificity of TSPO imaging in a rat model of peripherally-induced neuroinflammation. *Brain Behav Immun*. 2021;96:154-67.
93. Nutma E, Ceyzeriat K, Amor S, Tsartsalis S, Millet P, Owen DR, et al. Cellular sources of TSPO expression in healthy and diseased brain. *Eur J Nucl Med Mol Imaging*. 2021;49(1):146-63.
94. Sehlin D, Hultqvist G, Michno W, Aguilar X, Dahlén AD, Cerilli E, et al. Bispecific brain-penetrant antibodies for treatment of Alzheimer's disease. *J Prev Alzheimers Dis*. 2025:100214.
95. Schlepckow K. Therapeutic targeting of TREM2: A novel approach for treatment of AD? *Alzheimer's & Dementia*. 2023;19(S21):e072079.
96. Lameka K, Farwell MD, Ichise M. Positron Emission Tomography. *Handb Clin Neurol*. 2016;135:209-27.
97. Alauddin MM. Positron emission tomography (PET) imaging with ¹⁸F-based radiotracers. *Am J Nucl Med Mol Imaging*. 2012;2(1):55-76.
98. Basu S, Kwee TC, Surti S, Akin EA, Yoo D, Alavi A. Fundamentals of PET and PET/CT imaging. *Ann N Y Acad Sci*. 2011;1228:1-18.
99. Prenosil GA, Sari H, Fürstner M, Afshar-Oromieh A, Shi K, Rominger A, et al. Performance Characteristics of the Biograph Vision Quadra PET/CT System with a Long Axial Field of View Using the NEMA NU 2-2018 Standard. *J Nucl Med*. 2022;63(3):476-84.
100. Bailey DL HJ, Todd-Pokropek A, Aswegen A van. Nuclear Medicine Physics: A Handbook for Teachers and Students. Endorsed by: American Association of Physicists in Medicine (AAPM), Asia-Oceania Federation of Organizations for Medical Physics (AFOMP), Australasian College of Physical Scientists and Engineers in Medicine (ACPSEM), European Federation of Organisations for Medical Physics (EFOMP), Federation of African Medical Physics Organisations (FAMPO), World Federation of Nuclear Medicine and Biology (WFNMB): IAEA; 2014.
101. Hooker JM, Carson RE. Human Positron Emission Tomography Neuroimaging. *Annu Rev Biomed Eng*. 2019;21:551-81.
102. Patil S, Ayubcha C, Teichner E, Subtirelu R, Cho JH, Ghonim M, et al. Clinical Applications of PET Imaging in Alzheimer's Disease. *PET Clin*. 2025;20(1):89-100.
103. Bollack A, Pemberton HG, Collij LE, Markiewicz P, Cash DM, Farrar G, et al. Longitudinal amyloid and tau PET imaging in Alzheimer's disease: A systematic review of methodologies and factors affecting quantification. *Alzheimers Dement*. 2023;19(11):5232-52.
104. Chauveau F, Becker G, Boutin H. Have (R)-[¹¹C]PK11195 challengers fulfilled the promise? A scoping review of clinical TSPO PET studies. *Eur J Nucl Med Mol Imaging*. 2021;49(1):201-20.

105. Dupont AC, Largeau B, Santiago Ribeiro MJ, Guilloteau D, Tronel C, Arlicot N. Translocator Protein-18 kDa (TSPO) Positron Emission Tomography (PET) Imaging and Its Clinical Impact in Neurodegenerative Diseases. *Int J Mol Sci.* 2017;18(4).
106. Chauveau F, Boutin H, Van Camp N, Dollé F, Tavitian B. Nuclear imaging of neuroinflammation: a comprehensive review of [¹¹C]PK11195 challengers. *Eur J Nucl Med Mol Imaging.* 2008;35(12):2304-19.
107. Boutin H, Murray K, Pradillo J, Maroy R, Smigova A, Gerhard A, et al. ¹⁸F-GE-180: a novel TSPO radiotracer compared to ¹¹C-R-PK11195 in a preclinical model of stroke. *Eur J Nucl Med Mol Imaging.* 2015;42(3):503-11.
108. Fujita M, Kobayashi M, Ikawa M, Gunn RN, Rabiner EA, Owen DR, et al. Comparison of four ¹¹C-labeled PET ligands to quantify translocator protein 18 kDa (TSPO) in human brain: (R)-PK11195, PBR28, DPA-713, and ER176-based on recent publications that measured specific-to-non-displaceable ratios. *EJNMMI Res.* 2017;7(1):84.
109. Cumming P, Burgher B, Patkar O, Breakspear M, Vasdev N, Thomas P, et al. Sifting through the surfeit of neuroinflammation tracers. *J Cereb Blood Flow Metab.* 2018;38(2):204-24.
110. Yoder KK, Nho K, Risacher SL, Kim S, Shen L, Saykin AJ. Influence of TSPO genotype on ¹¹C-PBR28 standardized uptake values. *J Nucl Med.* 2013;54(8):1320-2.
111. Zhang L, Hu K, Shao T, Hou L, Zhang S, Ye W, et al. Recent developments on PET radiotracers for TSPO and their applications in neuroimaging. *Acta Pharm Sin B.* 2021;11(2):373-93.
112. Guilarte TR. TSPO in diverse CNS pathologies and psychiatric disease: A critical review and a way forward. *Pharmacol Ther.* 2019;194:44-58.
113. Gouilly D, Saint-Aubert L, Ribeiro MJ, Salabert AS, Tauber C, Péran P, et al. Neuroinflammation PET imaging of the translocator protein (TSPO) in Alzheimer's disease: An update. *Eur J Neurosci.* 2022;55(5):1322-43.
114. Zhang M, Qian XH, Hu J, Zhang Y, Lin X, Hai W, et al. Integrating TSPO PET imaging and transcriptomics to unveil the role of neuroinflammation and amyloid- β deposition in Alzheimer's disease. *Eur J Nucl Med Mol Imaging.* 2024;51(2):455-67.
115. Garland EF, Antony H, Kulagowska L, Scott T, Rogien C, Bottlaender M, et al. The microglial translocator protein (TSPO) in Alzheimer's disease reflects a phagocytic phenotype. *Acta Neuropathol.* 2024;148(1):62.
116. Chauveau F, Winkeler A, Chalon S, Boutin H, Becker G. PET imaging of neuroinflammation: any credible alternatives to TSPO yet? *Mol Psychiatry.* 2025;30(1):213-28.
117. Brendel M, Kleinberger G, Probst F, Jaworska A, Overhoff F, Blume T, et al. Increase of TREM2 during Aging of an Alzheimer's Disease Mouse Model Is Paralleled by Microglial Activation and Amyloidosis. *Front Aging Neurosci.* 2017;9:8.
118. Imai K, Takaoka A. Comparing antibody and small-molecule therapies for cancer. *Nat Rev Cancer.* 2006;6(9):714-27.
119. Boado RJ, Zhou QH, Lu JZ, Hui EK, Pardridge WM. Pharmacokinetics and brain uptake of a genetically engineered bifunctional fusion antibody targeting the mouse transferrin receptor. *Mol Pharm.* 2010;7(1):237-44.
120. Gustavsson T, Syvänen S, O'Callaghan P, Sehlin D. SPECT imaging of distribution and retention of a brain-penetrating bispecific amyloid- β antibody in a mouse model of Alzheimer's disease. *Transl Neurodegener.* 2020;9(1):37.
121. Hultqvist G, Syvänen S, Fang XT, Lannfelt L, Sehlin D. Bivalent Brain Shuttle Increases Antibody Uptake by Monovalent Binding to the Transferrin Receptor. *Theranostics.* 2017;7(2):308-18.
122. Lee HJ, Engelhardt B, Lesley J, Bickel U, Pardridge WM. Targeting rat anti-mouse transferrin receptor monoclonal antibodies through blood-brain barrier in mouse. *J Pharmacol Exp Ther.* 2000;292(3):1048-52.
123. Magnusson K, Sehlin D, Syvänen S, Svedberg MM, Philipson O, Söderberg L, et al. Specific uptake of an amyloid- β protofibril-binding antibody-tracer in A β PP transgenic mouse brain. *J Alzheimers Dis.* 2013;37(1):29-40.

124. Sehlin D, Fang XT, Cato L, Antoni G, Lannfelt L, Syvänen S. Antibody-based PET imaging of amyloid beta in mouse models of Alzheimer's disease. *Nat Commun.* 2016;7:10759.
125. Syvänen S, Hultqvist G, Gustavsson T, Gumucio A, Laudon H, Söderberg L, et al. Efficient clearance of A β protofibrils in A β PP-transgenic mice treated with a brain-penetrating bifunctional antibody. *Alzheimers Res Ther.* 2018;10(1):49.
126. Yu YJ, Zhang Y, Kenrick M, Hoyte K, Luk W, Lu Y, et al. Boosting brain uptake of a therapeutic antibody by reducing its affinity for a transcytosis target. *Sci Transl Med.* 2011;3(84):84ra44.
127. Jones AR, Shusta EV. Blood-brain barrier transport of therapeutics via receptor-mediation. *Pharm Res.* 2007;24(9):1759-71.
128. Yu YJ, Watts RJ. Developing therapeutic antibodies for neurodegenerative disease. *Neurotherapeutics.* 2013;10(3):459-72.
129. Meier SR, Sehlin D, Hultqvist G, Syvänen S. Pinpointing Brain TREM2 Levels in Two Mouse Models of Alzheimer's Disease. *Mol Imaging Biol.* 2021;23(5):665-75.
130. Shojaei M, Schaefer R, Schlepckow K, Kunze LH, Struebing FL, Brunner B, et al. PET imaging of microglia in Alzheimer's disease using copper-64 labeled TREM2 antibodies. *Theranostics.* 2024;14(16):6319-36.
131. Sehlin D, Fang XT, Meier SR, Jansson M, Syvänen S. Pharmacokinetics, biodistribution and brain retention of a bispecific antibody-based PET radioligand for imaging of amyloid- β . *Sci Rep.* 2017;7(1):17254.
132. Zeven K, Dierick H, Sevenois M, Baudhuin H, Navarro L, Van den Block S, et al. Optimizing antibody PET imaging: a comparative preclinical analysis of nanobody and minibody-like PET tracers. *Eur J Nucl Med Mol Imaging.* 2025.
133. Sehlin D, Syvänen S. Engineered antibodies: new possibilities for brain PET? *Eur J Nucl Med Mol Imaging.* 2019;46(13):2848-58.
134. Widera A, Norouziyan F, Shen WC. Mechanisms of TfR-mediated transcytosis and sorting in epithelial cells and applications toward drug delivery. *Adv Drug Deliv Rev.* 2003;55(11):1439-66.
135. Bien-Ly N, Yu YJ, Bumbaca D, Elstrott J, Boswell CA, Zhang Y, et al. Transferrin receptor (TfR) trafficking determines brain uptake of TfR antibody affinity variants. *J Exp Med.* 2014;211(2):233-44.
136. Pardridge WM, Boado RJ, Giugliani R, Schmidt M. Plasma Pharmacokinetics of Valanafusp Alpha, a Human Insulin Receptor Antibody-Iduronidase Fusion Protein, in Patients with Mucopolysaccharidosis Type I. *BioDrugs.* 2018;32(2):169-76.
137. Zhang W, Liu QY, Haqqani AS, Leclerc S, Liu Z, Fauteux F, et al. Differential expression of receptors mediating receptor-mediated transcytosis (RMT) in brain microvessels, brain parenchyma and peripheral tissues of the mouse and the human. *Fluids Barriers CNS.* 2020;17(1):47.
138. Jones AR, Stutz CC, Zhou Y, Marks JD, Shusta EV. Identifying blood-brain-barrier selective single-chain antibody fragments. *Biotechnol J.* 2014;9(5):664-74.
139. Rosa A, Metzendorf NG, Efverström J, Godec A, Sehlin D, Morrison J, et al. Lowering the affinity of single-chain monovalent BBB shuttle scFc-scFv8D3 prolongs its half-life and increases brain concentration. *Neurotherapeutics.* 2025;22(1):e00492.
140. Hersh AM, Alomari S, Tyler BM. Crossing the Blood-Brain Barrier: Advances in Nanoparticle Technology for Drug Delivery in Neuro-Oncology. *Int J Mol Sci.* 2022;23(8).
141. Zha S, Liu H, Li H, Li H, Wong KL, All AH. Functionalized Nanomaterials Capable of Crossing the Blood-Brain Barrier. *ACS Nano.* 2024;18(3):1820-45.
142. Hanson LR, Frey WH, 2nd. Intranasal delivery bypasses the blood-brain barrier to target therapeutic agents to the central nervous system and treat neurodegenerative disease. *BMC Neurosci.* 2008;9 Suppl 3(Suppl 3):S5.
143. Miyake MM, Bleier BS. The blood-brain barrier and nasal drug delivery to the central nervous system. *Am J Rhinol Allergy.* 2015;29(2):124-7.

144. Burgess A, Shah K, Hough O, Hynynen K. Focused ultrasound-mediated drug delivery through the blood-brain barrier. *Expert Rev Neurother*. 2015;15(5):477-91.
145. Rezaei AR, D'Haese PF, Finomore V, Carpenter J, Ranjan M, Wilhelmsen K, et al. Ultrasound Blood-Brain Barrier Opening and Aducanumab in Alzheimer's Disease. *N Engl J Med*. 2024;390(1):55-62.
146. Schlepckow K, Monroe KM, Kleinberger G, Cantuti-Castelvetri L, Parhizkar S, Xia D, et al. Enhancing protective microglial activities with a dual function TREM2 antibody to the stalk region. *EMBO Mol Med*. 2020;12(4):e11227.
147. Kariolis MS, Wells RC, Getz JA, Kwan W, Mahon CS, Tong R, et al. Brain delivery of therapeutic proteins using an Fc fragment blood-brain barrier transport vehicle in mice and monkeys. *Sci Transl Med*. 2020;12(545).
148. Lin M, Paolillo V, Le DB, Macapinlac H, Ravizzini GC. Monoclonal antibody based radiopharmaceuticals for imaging and therapy. *Curr Probl Cancer*. 2021;45(5):100796.
149. Hrynychak I, Cocioabă D, Fonseca AI, Leonte R, do Carmo SJC, Cornoiu R, et al. Antibody and Nanobody Radiolabeling with Copper-64: Solid vs. Liquid Target Approach. *Molecules*. 2023;28(12).
150. Braune A, Oehme L, Freudenberg R, Hofheinz F, van den Hoff J, Kotzerke J, et al. Comparison of image quality and spatial resolution between ^{18}F , ^{68}Ga , and ^{64}Cu phantom measurements using a digital Biograph Vision PET/CT. *EJNMMI Phys*. 2022;9(1):58.
151. Chomet M, van Dongen GAMS, Vugts DJ. State of the Art in Radiolabeling of Antibodies with Common and Uncommon Radiometals for Preclinical and Clinical Immuno-PET. *Bioconjug Chem*. 2021;32(7):1315-30.
152. Cooper MS, Ma MT, Sunassee K, Shaw KP, Williams JD, Paul RL, et al. Comparison of ^{64}Cu -complexing bifunctional chelators for radioimmunoconjugation: labeling efficiency, specific activity, and in vitro/in vivo stability. *Bioconjug Chem*. 2012;23(5):1029-39.
153. Price EW, Orvig C. Matching chelators to radiometals for radiopharmaceuticals. *Chem Soc Rev*. 2014;43(1):260-90.
154. Ghosh SC, Pinkston KL, Robinson H, Harvey BR, Wilganowski N, Gore K, et al. Comparison of DOTA and NODAGA as chelators for ^{64}Cu -labeled immunoconjugates. *Nucl Med Biol*. 2015;42(2):177-83.
155. Maisonia-Besset A, Witkowski T, Quintana M, Besse S, Gaumet V, Cordonnier A, et al. Synthesis and In Vitro Comparison of DOTA, NODAGA and 15-5 Macrocycles as Chelators for the ^{64}Cu -Labelling of Immunoconjugates. *Molecules*. 2022;28(1).
156. Morais M, Ma MT. Site-specific chelator-antibody conjugation for PET and SPECT imaging with radiometals. *Drug Discov Today Technol*. 2018;30:91-104.
157. Cheng Y, Lu J, Zhang C, Yan W, Zhu P, Qin Q, et al. Overview of antibody-drug conjugates nonclinical and clinical toxicities and related contributing factors. *Antib Ther*. 2025;8(2):124-44.
158. Elder GA, Gama Sosa MA, De Gasperi R. Transgenic mouse models of Alzheimer's disease. *Mt Sinai J Med*. 2010;77(1):69-81.
159. Zhong MZ, Peng T, Duarte ML, Wang M, Cai D. Updates on mouse models of Alzheimer's disease. *Mol Neurodegener*. 2024;19(1):23.
160. St George-Hyslop PH, Tanzi RE, Polinsky RJ, Haines JL, Nee L, Watkins PC, et al. The genetic defect causing familial Alzheimer's disease maps on chromosome 21. *Science*. 1987;235(4791):885-90.
161. Goldgaber D, Lerman MI, McBride OW, Saffiotti U, Gajdusek DC. Characterization and chromosomal localization of a cDNA encoding brain amyloid of Alzheimer's disease. *Science*. 1987;235(4791):877-80.
162. Tanzi RE, Gusella JF, Watkins PC, Bruns GA, St George-Hyslop P, Van Keuren ML, et al. Amyloid beta protein gene: cDNA, mRNA distribution, and genetic linkage near the Alzheimer locus. *Science*. 1987;235(4791):880-4.
163. Sherrington R, Rogaev EI, Liang Y, Rogaeva EA, Levesque G, Ikeda M, et al. Cloning of a gene bearing missense mutations in early-onset familial Alzheimer's disease. *Nature*. 1995;375(6534):754-60.

164. Rogaeve EI, Sherrington R, Rogaeve EA, Levesque G, Ikeda M, Liang Y, et al. Familial Alzheimer's disease in kindreds with missense mutations in a gene on chromosome 1 related to the Alzheimer's disease type 3 gene. *Nature*. 1995;376(6543):775-8.
165. Hardy J, Selkoe DJ. The amyloid hypothesis of Alzheimer's disease: progress and problems on the road to therapeutics. *Science*. 2002;297(5580):353-6.
166. Shen J, Kelleher RJ, 3rd. The presenilin hypothesis of Alzheimer's disease: evidence for a loss-of-function pathogenic mechanism. *Proc Natl Acad Sci U S A*. 2007;104(2):403-9.
167. Capecchi MR. Altering the genome by homologous recombination. *Science*. 1989;244(4910):1288-92.
168. Hall B, Limaye A, Kulkarni AB. Overview: generation of gene knockout mice. *Curr Protoc Cell Biol*. 2009;Chapter 19:Unit 19.2 .2.1-7.
169. Bhaya D, Davison M, Barrangou R. CRISPR-Cas systems in bacteria and archaea: versatile small RNAs for adaptive defense and regulation. *Annu Rev Genet*. 2011;45:273-97.
170. Drummond E, Wisniewski T. Alzheimer's disease: experimental models and reality. *Acta Neuropathol*. 2017;133(2):155-75.
171. Banik A, Brown RE, Bamberg J, Lahiri DK, Khurana D, Friedland RP, et al. Translation of Pre-Clinical Studies into Successful Clinical Trials for Alzheimer's Disease: What are the Roadblocks and How Can They Be Overcome? *J Alzheimers Dis*. 2015;47(4):815-43.
172. Cummings JL, Morstorf T, Zhong K. Alzheimer's disease drug-development pipeline: few candidates, frequent failures. *Alzheimers Res Ther*. 2014;6(4):37.
173. Welikovitsh LA, Mate de Gerando A, Khasnavis A, Bhavsar H, Meltzer JC, Buée L, et al. Tau, synapse loss and gliosis progress in an Alzheimer's mouse model after amyloid- β immunotherapy. *Brain*. 2025;148(4):1316-28.
174. Purro SA, Farmer M, Quarterman E, Ravey J, Thomas DX, Noble E, et al. Induction and characterisation of A β and tau pathology in *App^{NL-F/NL-F}* mice following inoculation with Alzheimer's disease brain homogenate. *bioRxiv*. 2024:2024.07.11.602448.
175. Rizzo SJS, Haynes KA, Santos DFS, Doolen S, Williams S-P, Little G, et al. Aging \times Genetics \times Environment: Characterization of Precision Disease Models for Preclinical Testing for Late-onset Alzheimer's disease. *Alzheimer's & Dementia*. 2023;19(S12):e072778.
176. Kotredes KP, Pandey RS, Persohn S, Elderidge K, Burton CP, Miner EW, et al. Characterizing Molecular and Synaptic Signatures in mouse models of Late-Onset Alzheimer's Disease Independent of Amyloid and Tau Pathology. *bioRxiv*. 2023:2023.12.19.571985.
177. Richard BC, Kurdakova A, Baches S, Bayer TA, Weggen S, Wirths O. Gene Dosage Dependent Aggravation of the Neurological Phenotype in the 5XFAD Mouse Model of Alzheimer's Disease. *J Alzheimers Dis*. 2015;45(4):1223-36.
178. Jawhar S, Trawicka A, Jenneckens C, Bayer TA, Wirths O. Motor deficits, neuron loss, and reduced anxiety coinciding with axonal degeneration and intraneuronal A β aggregation in the 5XFAD mouse model of Alzheimer's disease. *Neurobiol Aging*. 2012;33(1):196.e29-40.
179. Forner S, Kawauchi S, Balderrama-Gutierrez G, Kramár EA, Matheos DP, Phan J, et al. Systematic phenotyping and characterization of the 5xFAD mouse model of Alzheimer's disease. *Sci Data*. 2021;8(1):270.
180. Sasmita AO, Ong EC, Nazarenko T, Mao S, Komarek L, Thalmann M, et al. Parental origin of transgene modulates amyloid- β plaque burden in the 5xFAD mouse model of Alzheimer's disease. *Neuron*. 2025;113(6):838-46.e4.
181. Xia D, Lianoglou S, Sandmann T, Calvert M, Suh JH, Thomsen E, et al. Novel *App* knock-in mouse model shows key features of amyloid pathology and reveals profound metabolic dysregulation of microglia. *Mol Neurodegener*. 2022;17(1):41.
182. Gillings N, Hjelstuen O, Ballinger J, Behe M, Decristoforo C, Elsinga P, et al. Guideline on current good radiopharmacy practice (cGRPP) for the small-scale preparation of radiopharmaceuticals. *EJNMMI Radiopharm Chem*. 2021;6(1):8.

183. Stortz G, Thiessen JD, Bishop D, Khan MS, Kozlowski P, Retière F, et al. Performance of a PET Insert for High-Resolution Small-Animal PET/MRI at 7 Tesla. *J Nucl Med.* 2018;59(3):536-42.
184. Rosar F, Buchholz HG, Michels S, Hoffmann MA, Piel M, Waldmann CM, et al. Image quality analysis of ⁴⁴Sc on two preclinical PET scanners: a comparison to ⁶⁸Ga. *EJNMMI Phys.* 2020;7(1):16.
185. Moses WW. Fundamental Limits of Spatial Resolution in PET. *Nucl Instrum Methods Phys Res A.* 2011;648 Supplement 1:S236-s40.
186. van Sluis J, de Jong J, Schaar J, Noordzij W, van Snick P, Dierckx R, et al. Performance Characteristics of the Digital Biograph Vision PET/CT System. *J Nucl Med.* 2019;60(7):1031-6.
187. Øen SK, Aasheim LB, Eikenes L, Karlberg AM. Image quality and detectability in Siemens Biograph PET/MRI and PET/CT systems-a phantom study. *EJNMMI Phys.* 2019;6(1):16.
188. Lue LF, Schmitz CT, Serrano G, Sue LI, Beach TG, Walker DG. TREM2 Protein Expression Changes Correlate with Alzheimer's Disease Neurodegenerative Pathologies in Post-Mortem Temporal Cortices. *Brain Pathol.* 2015;25(4):469-80.
189. Diaz-Lucena D, Kruse N, Thüne K, Schmitz M, Villar-Piqué A, da Cunha JEG, et al. TREM2 expression in the brain and biological fluids in prion diseases. *Acta Neuropathol.* 2021;141(6):841-59.
190. Quach S, Holzgreve A, Kaiser L, Unterrainer M, Dekorsy FJ, Nelwan DV, et al. TSPO PET signal using [(18)F]GE180 is associated with survival in recurrent gliomas. *Eur J Nucl Med Mol Imaging.* 2023;50(3):859-69.
191. Bartos LM, Kirchleitner SV, Kolabas ZI, Quach S, Beck A, Lorenz J, et al. Deciphering sources of PET signals in the tumor microenvironment of glioblastoma at cellular resolution. *Sci Adv.* 2023;9(43):eadi8986.
192. Kuntner C, Stout DB. Quantitative preclinical PET imaging: opportunities and challenges. *Front Phys.* 2014;Volume 2 - 2014.
193. Mortazi A, Udupa JK, Odhner D, Tong Y, Torigian DA. Post-acquisition Standardization of Positron Emission Tomography Images. *Res Sq.* 2023.
194. Kinahan PE, Fletcher JW. Positron emission tomography-computed tomography standardized uptake values in clinical practice and assessing response to therapy. *Semin Ultrasound CT MR.* 2010;31(6):496-505.
195. Summerfield SG, Yates JWT, Fairman DA. Free Drug Theory - No Longer Just a Hypothesis? *Pharm Res.* 2022;39(2):213-22.
196. Webborn PJH, Beaumont K, Martin IJ, Smith DA. Free Drug Concepts: A Lingering Problem in Drug Discovery. *J Med Chem.* 2025;68(7):6850-6.
197. Keyes JW, Jr. SUV: standard uptake or silly useless value? *J Nucl Med.* 1995;36(10):1836-9.
198. Huang SC. Anatomy of SUV. Standardized uptake value. *Nucl Med Biol.* 2000;27(7):643-6.
199. Gunn RN, Gunn SR, Cunningham VJ. Positron emission tomography compartmental models. *J Cereb Blood Flow Metab.* 2001;21(6):635-52.
200. Su Y, Vlassenko AG, Couture LE, Benzinger TL, Snyder AZ, Derdeyn CP, et al. Quantitative hemodynamic PET imaging using image-derived arterial input function and a PET/MR hybrid scanner. *J Cereb Blood Flow Metab.* 2017;37(4):1435-46.
201. Zanotti-Fregonara P, Chen K, Liow JS, Fujita M, Innis RB. Image-derived input function for brain PET studies: many challenges and few opportunities. *J Cereb Blood Flow Metab.* 2011;31(10):1986-98.
202. Volpi T, Maccioni L, Colpo M, Debiasi G, Capotosti A, Ciceri T, et al. An update on the use of image-derived input functions for human PET studies: new hopes or old illusions? *EJNMMI Res.* 2023;13(1):97.
203. Buchert R, Dirks M, Schütze C, Wilke F, Mamach M, Wirries A-K, et al. Reliable quantification of 18F-GE-180 PET neuroinflammation studies using an individually scaled population-based input function or late tissue-to-blood ratio. *Eur J Nucl Med Mol Imaging.* 2020;47(12):2887-900.
204. James ML, Belichenko NP, Shuhendler AJ, Hoehne A, Andrews LE, Condon C, et al. [¹⁸F]GE-180 PET Detects Reduced Microglia Activation After LM11A-31 Therapy in a Mouse Model of Alzheimer's Disease. *Theranostics.* 2017;7(6):1422-36.

205. van Lengerich B, Zhan L, Xia D, Chan D, Joy D, Park JI, et al. A TREM2-activating antibody with a blood-brain barrier transport vehicle enhances microglial metabolism in Alzheimer's disease models. *Nat Neurosci.* 2023;26(3):416-29.
206. Anderson CJ, Connett JM, Schwarz SW, Rocque PA, Guo LW, Philpott GW, et al. Copper-64-labeled antibodies for PET imaging. *J Nucl Med.* 1992;33(9):1685-91.
207. Badier L, Quelves I. Zirconium 89 and Copper 64 for ImmunoPET: From Antibody Bioconjugation and Radiolabeling to Molecular Imaging. *Pharmaceutics.* 2024;16(7).
208. Trautwein NF, Schwenck J, Seitz C, Seith F, Calderón E, von Beschwitz S, et al. A novel approach to guide GD2-targeted therapy in pediatric tumors by PET and [(64)Cu]Cu-NOTA-ch14.18/CHO. *Theranostics.* 2024;14(3):1212-23.
209. Brady ED, Chong HS, Milenic DE, Brechbiel MW. Development of a spectroscopic assay for bifunctional ligand-protein conjugates based on copper. *Nucl Med Biol.* 2004;31(6):795-802.
210. Gallagher SR. One-dimensional SDS gel electrophoresis of proteins. *Curr Protoc Immunol.* 2006;Chapter 8:Unit 8.4.
211. Bird IM. High performance liquid chromatography: principles and clinical applications. *Bmj.* 1989;299(6702):783-7.
212. Johnston RF, Pickett SC, Barker DL. Autoradiography using storage phosphor technology. *Electrophoresis.* 1990;11(5):355-60.
213. Ishiwata K, Ogi N, Tanaka A, Senda M. Quantitative ex vivo and in vitro receptor autoradiography using ¹¹C-labeled ligands and an imaging plate: a study with a dopamine D₂-like receptor ligand [¹¹C]nemonapride. *Nucl Med Biol.* 1999;26(3):291-6.
214. Bader AS, Gnädig MU, Fricke M, Büschgens L, Berger LJ, Klafki HW, et al. Brain Region-Specific Differences in Amyloid-β Plaque Composition in 5XFAD Mice. *Life (Basel).* 2023;13(4).
215. Boeddrich A, Haenig C, Neuendorf N, Blanc E, Ivanov A, Kirchner M, et al. A proteomics analysis of 5xFAD mouse brain regions reveals the lysosome-associated protein Arl8b as a candidate biomarker for Alzheimer's disease. *Genome Med.* 2023;15(1):50.
216. Price BR, Sudduth TL, Weekman EM, Johnson S, Hawthorne D, Woolums A, et al. Therapeutic Trem2 activation ameliorates amyloid-beta deposition and improves cognition in the 5XFAD model of amyloid deposition. *J Neuroinflammation.* 2020;17(1):238.
217. Oakley H, Cole SL, Logan S, Maus E, Shao P, Craft J, et al. Intraneuronal beta-amyloid aggregates, neurodegeneration, and neuron loss in transgenic mice with five familial Alzheimer's disease mutations: potential factors in amyloid plaque formation. *J Neurosci.* 2006;26(40):10129-40.
218. Ovacik M, Lin K. Tutorial on Monoclonal Antibody Pharmacokinetics and Its Considerations in Early Development. *Clin Transl Sci.* 2018;11(6):540-52.
219. Awwad S, Angkawitwong U. Overview of Antibody Drug Delivery. *Pharmaceutics.* 2018;10(3).
220. Xenaki KT, Oliveira S, van Bergen En Henegouwen PMP. Antibody or Antibody Fragments: Implications for Molecular Imaging and Targeted Therapy of Solid Tumors. *Front Immunol.* 2017;8:1287.
221. Syvänen S, Fang XT, Hultqvist G, Meier SR, Lannfelt L, Sehlin D. A bispecific Tribody PET radioligand for visualization of amyloid-beta protofibrils - a new concept for neuroimaging. *Neuroimage.* 2017;148:55-63.
222. James ML, Belichenko NP, Nguyen TV, Andrews LE, Ding Z, Liu H, et al. PET Imaging of Translocator Protein (18 kDa) in a Mouse Model of Alzheimer's Disease Using N-(2,5-Dimethoxybenzyl)-2-¹⁸F-fluoro-N-(2-Phenoxyphenyl)Acetamide. *J Nucl Med.* 2015;56(2):311-6.
223. Chaney A, Cropper HC, Johnson EM, Lechtenberg KJ, Peterson TC, Stevens MY, et al. ¹¹C-DPA-713 Versus ¹⁸F-GE-180: A Preclinical Comparison of Translocator Protein 18 kDa PET Tracers to Visualize Acute and Chronic Neuroinflammation in a Mouse Model of Ischemic Stroke. *J Nucl Med.* 2019;60(1):122-8.
224. Liu Y, Xu Y, Li M, Pan D, Li Y, Wang Y, et al. Multi-target PET evaluation in APP/PS1/tau mouse model of Alzheimer's disease. *Neurosci Lett.* 2020;728:134938.

225. Vignal N, Cisternino S, Rizzo-Padoin N, San C, Hontonnou F, Gelé T, et al. [¹⁸F]FEPPA a TSPO Radioligand: Optimized Radiosynthesis and Evaluation as a PET Radiotracer for Brain Inflammation in a Peripheral LPS-Injected Mouse Model. *Molecules*. 2018;23(6).
226. Liu SY, Qiao HW, Song TB, Liu XL, Yao YX, Zhao CS, et al. Brain microglia activation and peripheral adaptive immunity in Parkinson's disease: a multimodal PET study. *J Neuroinflammation*. 2022;19(1):209.
227. Wang Q, Chen G, Schindler SE, Christensen J, McKay NS, Liu J, et al. Baseline Microglial Activation Correlates With Brain Amyloidosis and Longitudinal Cognitive Decline in Alzheimer Disease. *Neurol Neuroimmunol Neuroinflamm*. 2022;9(3).
228. Cheng MF, Cheng TJ, Guo YL, Chiu CH, Wu HM, Yen RF, et al. Neuroinflammation in Low-Level PM2.5-Exposed Rats Illustrated by PET via an Improved Automated Produced [¹⁸F]FEPPA: A Feasibility Study. *Mol Imaging*. 2022;2022:1076444.
229. López-Picón FR, Keller T, Bocancea D, Helin JS, Krzyczmonik A, Helin S, et al. Direct Comparison of [¹⁸F]F-DPA with [¹⁸F]DPA-714 and [¹¹C]PBR28 for Neuroinflammation Imaging in the same Alzheimer's Disease Model Mice and Healthy Controls. *Mol Imaging Biol*. 2022;24(1):157-66.
230. Bartos LM, Kunte ST, Beumers P, Xiang X, Wind K, Ziegler S, et al. Single-Cell Radiotracer Allocation via Immunomagnetic Sorting to Disentangle PET Signals at Cellular Resolution. *J Nucl Med*. 2022;63(10):1459-62.
231. Xiang X, Wind K, Wiedemann T, Blume T, Shi Y, Briel N, et al. Microglial activation states drive glucose uptake and FDG-PET alterations in neurodegenerative diseases. *Sci Transl Med*. 2021;13(615):eabe5640.
232. Hopperton KE, Mohammad D, Trépanier MO, Giuliano V, Bazinet RP. Markers of microglia in post-mortem brain samples from patients with Alzheimer's disease: a systematic review. *Mol Psychiatry*. 2018;23(2):177-98.
233. Haass C, Kleinberger G, Schlepckow K. TREM2 cleavage modulators and uses thereof. WO2018015573A2. 2018.
234. Wang Y, Ulland TK, Ulrich JD, Song W, Tzaferis JA, Hole JT, et al. TREM2-mediated early microglial response limits diffusion and toxicity of amyloid plaques. *J Exp Med*. 2016;213(5):667-75.
235. Yuan P, Condello C, Keene CD, Wang Y, Bird TD, Paul SM, et al. TREM2 Haplodeficiency in Mice and Humans Impairs the Microglia Barrier Function Leading to Decreased Amyloid Compaction and Severe Axonal Dystrophy. *Neuron*. 2016;90(4):724-39.
236. Schaefer R, Kunze LH, Haertel M, Zhu Y, Schlepckow K, Willem M, et al. Image-Derived Blood Normalization of Antibody-Based TREM2 PET in Mouse Models of Amyloidosis and Myocardial Infarction. *J Nucl Med*. 2025.
237. Cui H, Banerjee S, Xie N, Hussain M, Jaiswal A, Liu H, et al. TREM2 promotes lung fibrosis via controlling alveolar macrophage survival and pro-fibrotic activity. *Nat Commun*. 2025;16(1):1761.
238. Piollet M, Porsch F, Rizzo G, Kapser F, Schulz DJJ, Kiss MG, et al. TREM2 protects from atherosclerosis by limiting necrotic core formation. *Nat Cardiovasc Res*. 2024;3(3):269-82.
239. Shi D, Si Z, Xu Z, Cheng Y, Lin Q, Fu Z, et al. Synthesis and Evaluation of ⁶⁸Ga-NOTA-COG1410 Targeting to TREM2 of TAMs as a Specific PET Probe for Digestive Tumor Diagnosis. *Anal Chem*. 2022;94(9):3819-30.
240. Turnbull IR, Gilfillan S, Cella M, Aoshi T, Miller M, Piccio L, et al. Cutting edge: TREM-2 attenuates macrophage activation. *J Immunol*. 2006;177(6):3520-4.
241. Sawiak SJ, Wood NI, Williams GB, Morton AJ, Carpenter TA. SPMMouse: A new toolbox for SPM in the animal brain. Paper presented at: ISMRM 17th Scientific Meeting & Exhibition, April, 2009.
242. Giavarina D. Understanding Bland Altman analysis. *Biochem Med (Zagreb)*. 2015;25(2):141-51.
243. Michael LH, Entman ML, Hartley CJ, Youker KA, Zhu J, Hall SR, et al. Myocardial ischemia and reperfusion: a murine model. *Am J Physiol*. 1995;269(6 Pt 2):H2147-54.
244. Jung SH, Hwang BH, Shin S, Park EH, Park SH, Kim CW, et al. Spatiotemporal dynamics of macrophage heterogeneity and a potential function of Trem2^{hi} macrophages in infarcted hearts. *Nat Commun*. 2022;13(1):4580.

-
245. Rizzo G, Gropper J, Piollet M, Vafadarnejad E, Rizakou A, Bandi SR, et al. Dynamics of monocyte-derived macrophage diversity in experimental myocardial infarction. *Cardiovasc Res.* 2023;119(3):772-85.
246. De Villiers C, Riley PR. Mouse models of myocardial infarction: comparing permanent ligation and ischaemia-reperfusion. *Dis Model Mech.* 2020;13(11).

8. List of Figures

Figure 1. Schematic illustration of a bispecific antibody (anti-TfR1 and anti-TREM2) crossing the BBB. ...	13
Figure 2. Graphical Abstract of the doctoral thesis. A visual representation of the application, validation and optimization of the TREM2 PET methodology. Created with BioRender.com.....	21
Figure 3. In vitro autoradiography of a representative AD mouse brain (5xFAD;TfR ^{mu/hu}) vs. a blocked control and pathology-free WT control. Red arrows highlight the cortex. Adapted from (130), licensed under CC BY 4.0.	23
Figure 4. Average TREM2 PET images 20 h p.i. of AD mouse brains vs. WT controls harboring the hTfR for the brain shuttle system (5xFAD;TfR ^{mu/hu} and WT;TfR ^{mu/hu}) and without the brain shuttle (5xFAD and WT). Red arrows indicate the cortex and hippocampus. Adapted from (130), licensed under CC BY 4.0.	23
Figure 5. Method Box 1. PET image processing workflow.	24
Figure 6. Radioligand uptake in perfused brains at 20 h p.i. One-way ANOVA/Tukey's multiple comparison test, $p < 0.01$ (**). Adapted from (130), licensed under CC BY 4.0.	25
Figure 7. Radioligand uptake in the cortex of the brain 20 h p.i. after perfusion. One-way ANOVA/Tukey's multiple comparison test, $p < 0.01$ (**). Adapted from (130), licensed under CC BY 4.0.	26
Figure 8. Ex vivo autoradiography of a representative AD mouse brain (5xFAD;TfR ^{mu/hu}) vs. WT control, 20 h p.i. and after perfusion. Red arrows mark the cortex. Adapted from (130), licensed under CC BY 4.0.	27
Figure 9. Radioactivity measurements per single cell in the microglia (cluster of differentiation 11b, CD11b) enriched and depleted fractions. (Microglia blue, neurons yellow, astrocytes pink, oligodendrocytes gray). Adapted from (130), licensed under CC BY 4.0. Created with BioRender.com. ...	27
Figure 10. Method Box 2. Workflow of scRadiotracing. Created with BioRender.com.....	28
Figure 11. Representative TREM2 immunohistochemistry and in vitro autoradiography as well as blocked in vitro autoradiography of a human brain section from an AD patient. Adapted from (130), licensed under CC BY 4.0.	28
Figure 12. The figure illustrates the volumes-of-interest (VOIs) utilized for blood segmentation from the heart. Manual segmentation of PET images using a spherical VOI. SPM-derived VOI employed in a data-driven approach to segment radioactivity levels from the blood. A significant correlation between blood samples of WT and TREM2 KO mice ($n = 11$ each) obtained ex vivo following PET imaging and the segmented blood radioactivity levels derived from PET utilizing a data-driven approach. Linear regression, 95% confidence interval. Adapted from (236), licensed under CC BY 4.0.	30
Figure 13. Method Box 3. SPM applications used in this study. Created with BioRender.com.....	31
Figure 14. SPM maps were generated for group comparisons between WT and TREM2 KO mice ($n = 11$ each) of TREM2 PET images after normalization to blood levels and %ID, and overlaid onto a CT template. Two-sample t-test, $p < 0.05$. Adapted from (236), licensed under CC BY 4.0.	32
Figure 15. Schematic illustration of segmented organs. And a relative TREM2 comparison of SPM t-values of these organs, representing the difference of the group comparison between WT and TREM2 KO mice ($n = 11$ each) and quantified TREM2 protein levels in WT mice ($n = 3$) by MSD analysis. Mean \pm SD. Adapted from (236), licensed under CC BY 4.0.	32
Figure 16. SPM maps were generated from group comparisons between WT;TfR ^{mu/hu} and APP ^{SAA} ;TfR ^{mu/hu} mice ($n = 6$ each) of TREM2 PET images after normalization to blood levels and overlaid on an MRI template. Two-sample t-test, $p < 0.05$. Representative ex vivo autoradiography of a perfused APP ^{SAA} ;TfR ^{mu/hu} brain slice and immunohistochemistry of the adjacent brain slice (DNA (4',6-Diamidin-2-	

<i>phenylindol, DAPI) in blue, microglia (ionized calcium-binding adapter molecule 1, Iba1) in yellow and TREM2 in red). Red arrows indicate increased TREM2 signals. Adapted from (236), licensed under CC BY 4.0.</i>	33
Figure 17. <i>Representative PET images (overlaid onto a CT) and correlating autoradiography images of the infarct region in the heart of a left anterior descending artery-(LAD)-ligated WT mouse (myocardial infarction model) and the same region in the heart of a sham-operated WT mouse. Illustrations show the planes of the images and are shown for orientation. Created with BioRender.com. Adapted from (236), licensed under CC BY 4.0.</i>	34

9. List of Tables

<i>Table 1. Overview of potential alternative strategies to improve BBB penetration for antibody-based radioligands.</i>	<i>14</i>
<i>Table 2. Contributions to paper I.</i>	<i>42</i>

10. Paper I

Monireh Shojaei, Rebecca Schaefer, Kai Schlepckow, Lea H. Kunze, Felix L. Struebing, Bettina Brunner, Michael Willem, Laura M. Bartos, Astrid Feiten, Giovanna Palumbo, Thomas Arzberger, Peter Bartenstein, Gian C. Parico, Dan Xia, Kathryn M. Monroe, Christian Haass, Matthias Brendel, Simon Lindner: **PET imaging of microglia in Alzheimer's disease using copper-64 labeled TREM2 antibodies**

Theranostics, 2024, doi: 10.7150/thno.97149

Licensed under Creative Commons Attribution 4.0 International License (CC BY 4.0, <https://creativecommons.org/licenses/by/4.0/>).

11. Paper II

Rebecca Schaefer, Lea H. Kunze, Marlies Haertel, Yeqian Zhu, Kai Schlepckow, Michael Willem, Laura M. Bartos, Giovanna Palumbo, Lukas Tomas, Christian Schulz, Steffen Massberg, Rudolf A. Werner, Maximilian Fischer, Dan Xia, Kathryn M. Monroe, Christian Haass, Matthias Brendel, Simon Lindner: **Image-Derived Blood Normalization of Antibody-Based TREM2 PET in Mouse Models of Amyloidosis and Myocardial Infarction**

Journal of Nuclear Medicine, 2025, doi: 10.2967/jnumed.125.269472

Licensed under Creative Commons Attribution 4.0 International License (CC BY 4.0, <https://creativecommons.org/licenses/by/4.0/>).

Danksagung

Zunächst möchte ich meinem Doktorvater, Priv.-Doz. Dr. Simon Lindner, meinen herzlichen Dank aussprechen. Seine kontinuierliche Förderung und sein Vertrauen in meine Arbeit haben mich sehr ermutigt. Mir wurde stets der Freiraum gegeben, eigene Forschungswege zu verfolgen, und er stand mir bei Fragen und Herausforderungen beratend zur Seite. Die Promotionszeit war für mich eine prägende Erfahrung, in der ich sehr viel gelernt habe und die ich in guter Erinnerung behalten werde.

Mein besonderer Dank gilt auch Prof. Dr. Dr. Matthias Brendel, dessen großzügige Unterstützung sowie engagierte und wohlwollende Förderung maßgeblich zu dieser Arbeit beigetragen haben.

Herrn Prof. Dr. Bartenstein, Herrn Prof. Dr. Dr. Matthias Brendel und Herrn Prof. Dr. Rudolf Werner danke ich herzlich für die Möglichkeit, meine Promotion an der Klinik und Poliklinik für Nuklearmedizin durchführen zu dürfen, Weiterbildungen zu absolvieren und an zahlreichen Kongressen auf nationaler und internationaler Ebene teilzunehmen.

Des Weiteren gilt mein Dank der DGN, iSRS und Synergy für die großzügige finanzielle Unterstützung in Form von Stipendien, die es mir ermöglichte, an Fortbildungen teilzunehmen und Kongresse zu besuchen.

Mein aufrichtiger Dank gilt auch meinen Kolleginnen und Kollegen, die mich während meiner Projekte tatkräftig unterstützt haben. Insbesondere danke ich Rosel Oos und Giovanna Palumbo, die mir bei allen Belangen rund um die Versuchstiere stets den Rücken freigehalten und eine angenehme Arbeitsatmosphäre geschaffen haben. Ein herzliches Dankeschön geht auch an das Helmholtz-Zentrum Dresden-Rossendorf und die Universität Tübingen, die mich wöchentlich mit Kupfer-64 versorgten, stellvertretend genannt Walter Ehrlichmann, Dr. Martin Kreller und Prof. Dr. Gerald Reischl. Dank gilt auch Prof. Dr. Dr. h.c. Christian Haass und Dr. Kai Schlepckow für ihre hilfreichen Kommentare zu den Manuskripten und inspirierenden fachlichen Austausch. Kathryn Monroe, Ph.D., und Dan Xia, Ph.D., danke ich für die Bereitstellung der Antikörper und die reibungslose Zusammenarbeit, sowie Monireh Shojaei für ihre Vorarbeit zur Radioligandenentwicklung. Dr. med. Felix Strübing möchte ich für die rekordverdächtig schnelle Etablierung der Histologie danken. Mein Dank gilt außerdem dem Team der Kardiologie, insbesondere Dr. med. Maximilian Fischer und Yeqian Zhu, für die konstruktive und produktive Zusammenarbeit.

Bedanken möchte ich mich aber auch bei allen, die mich an ihren Projekten haben mitarbeiten lassen und mir Einblicke in andere Forschungsgebiete ermöglicht haben. Mein besonderer Dank gilt hier Dr. Melissa Antons und Prof. Dr. Clemens Cyran aus der Klinik und Poliklinik für Radiologie am LMU Klinikum sowie Adrian Kromer und Prof. Dr. Olivia Merkel aus der Pharmazeutischen Technologie der LMU München. Mein besonderer Dank gilt außerdem Prof. Tuomas Knowles und Charlotte Fischer vom Department of Biophysics & Biophysical Chemistry der University of Cambridge, die mir die außergewöhnliche Gelegenheit ermöglicht haben, im Rahmen

eines Gastaufenthalts ihr Labor kennenzulernen. Es war eine bereichernde Erfahrung, für die ich sehr dankbar bin.

Ein weiterer besonders großer Dank gilt allen Kolleginnen und Kollegen der Klinik und Poliklinik für Nuklearmedizin, die mir jederzeit mit Rat und Tat zur Seite standen, mir viele bereichernde Momente ermöglichten und deren Türen - im wahrsten Sinne des Wortes - offenstanden. Ich bin für die vielen Teachings, Tipps, die entgegengebrachte Geduld und Unterstützung sehr dankbar. Ein herzlicher Dank gilt an der Stelle Prof. Dr. Guido Böning, Dr. Astrid Delker, Dr. Gabriel Sheikh, Dr. Mathias Zacherl und Prof. Dr. Sibylle Ziegler. Besonders hervorheben möchte ich Dr. Franz-Josef Gildehaus, der mich mit seiner Expertise und Hilfsbereitschaft stets unterstützt hat und sich über meine Fortschritte mit mir gefreut hat.

Dem Team der Radiopharmazie danke ich für die schöne gemeinsame Zeit. Es war mir nicht nur eine Ehre, sondern auch eine große Freude, Teil eures Teams zu sein. Besonders bedanken möchte ich mich bei Andreas Harbach, Benjamin Kugelmann, Marcel Simmet und Daniel Werner für die lustigen Momente und Ablenkungen, besonders in den forschungsintensiveren Phasen. Dr. Felix Lindheimer und Dr. Johannes Toms danke ich für die vielen hilfreichen Ratschläge, das geduldige Zuhören, die tatkräftige Unterstützung und die gemeinsamen Mittagspausen.

Mein Dank gilt auch Isabelle Fuxjäger, Marlies Härtel, Lea Kunze, Manvir Lalia und Sandra Resch für die Freundschaft, die während der Promotionszeit entstanden ist, und für mich zu den schönsten Erinnerungen dieser Zeit zählt. Danke für die Unterstützung, Ratschläge und Ermutigungen, die mir sehr viel bedeutet haben.

Hannah Aksungur, Charlotte Fischer, Lea Filipova, Benedikt Greck und Viktoria Kirst danke ich für ihre ehrliche Kritik, ihre treue Wegbegleitung und die Freundschaft, die mir eine große Stütze war und ist.

Von ganzem Herzen danke ich meinen Eltern und Geschwistern, die mich wie schon immer in allen Belangen unterstützt haben.

Abschließend möchte ich mich einfach nur bei Euch allen bedanken, dass Ihr mich auf diesem Weg begleitet und unterstützt habt. Ihr habt meine Promotionszeit bereichert und diese Arbeit erst möglich gemacht.

Danke